Title
ULTRARELRTIVISTIC NUCLEAR PHYSICS: FROM BECOMING TO BEING

Authors
W.M
Geist

Publication Date
1988-11-01

Lawrence Berkeley Laboratory
UNIVERSITY OF CALIFORNIA

Submitted to International Journal of Modern Physics A

Ultrarelativistic Nuclear Physics: From Becoming to Being

W.M. Geist

November 1988

NUCLEAR SCIENCE DIVISION

Prepared for the U.S. Department of Energy under Contract Number DE-AC03-76SF00098.

Ultrarelativistic Nuclear Physics:

from Becoming to Being

W.M. Geist

Nuclear Science Division
Lawrence Berkeley Laboratory
1 Cyclotron Road
Berkeley, California 94720

ABSTRACT

Basic theoretical ideas on a phase transition in heavy ion collisions to a thermalized plasma of free quarks and gluons are outlined. Major experiments are then described which made use of oxygen and sulphur beams with moderate (BNL) or high (CERN) momenta. Representative results pertaining to both average event features and quark-gluon plasma properties are discussed in some detail. This review addresses also interested non-specialists.

This work was supported by the Director, Office of Energy Research, Office of High Energy and Nuclear Physics, Nuclear Physics Division of the of the U.S. Department of Energy under Contract DE-AC03-76SF00098.

1. INTRODUCTION

Any experiment dealing with collisions of particles may be characterized by i) the number n_F of incoming elementary fermions (e.g., n_F = 2 (6) for e^+e^- (pp) interactions), ii) the invariant center-of-mass (cms) energy $\sqrt{s}$ and iii) the number N_{ev} of useful events recorded. In this framework current experiments with ion beams and heavy nuclear targets are easily seen to differ from cosmic ray experiments by much larger values of N_{ev}, from LBL and Dubna experiments due to higher $\sqrt{s}$, and from high energy elementary particle experiments due to the range of n_F: Collisions of sulfur ions with lead targets correspond to n_F=720 valence quarks, whereas n_F=1248 will be reached with lead beams on lead targets at CERN after 1991 and n_F=1182 for gold on gold collisions at RHIC a little later.

From this classification it is clear that there is little overlap with previous experience. It signals, therefore, the beginning of a new field of research. The large number of valence quarks (and gluons) involved suggests the name of the game: one is aiming at an investigation of thermodynamical behavior of strongly interacting matter, in particular of gluons and quarks.

Those not (yet) used to such ideas are asked to listen to Lucretius[1]:

> ...A new aspect of the Universe is striving to reveal itself...
> But no fact is so simple that it is not harder to believe than
> to doubt at the first presentation.

And indeed, a phase of free quarks and gluons (Quark-Gluon Plasma, QGP) has most probably filled the early universe at an age of less than 10^{-5} sec. Whether this QGP has left some observable traces is still an open question. Recent theoretical work suggests that it could help solving the dark matter problem.[2]

At this point it is appropriate to understand the motivation behind this new experimental program concerned with strong interactions. The present theory of strong interactions, QCD, explains virtually all features of deep inelastic processes of quasi-free partons on a rather satisfying level. However, the phenomenon of confinement of colored partons is not yet understood. It is this aspect that is addressed by heavy ion physics at high energies. In these collisions a phase transition is expected to occur, such that bound quarks and gluons become deconfined. Eventually, they would transform back into hadrons at a later stage. Hence deconfinement-confinement transitions may be studied in a 'controlled' way. The same idea may be viewed in a different way: The vacuum exerts a pressure on colored partons thus confining them to a small 'bag' in space, i.e. to uncolored hadrons. In collisions of nuclei 'macroscopic' regions of space may be filled, via a phase transition, by a QGP. The well proven macroscopic concepts of thermo- and hydrodynamics ought to be applicable to this situation. This should then ease the task of understanding the coexistence of the QGP with the surrounding QCD vacuum, i.e. with the ground state of the theory.

In the following section 2, basic theoretical concepts concerning the QGP plasma will be introduced on an intuitive level . More complete theoretical accounts can be found in refs. 3,4. Major present experiments are briefly described in section 3. Data on typical event properties are discussed in section 4. First measurements of quantities which are predicted to be directly related to the QGP are presented in section 5, together with more theoretical details. No attempt was made to compile a vast amount of data; instead, a limited number of representative measurements available in early summer 1988 was selected. The current understanding of nuclear collisions at very high energies is summarized in the concluding section 6.

2. THEORETICAL CONCEPTS

2.1 Thermodynamics

In pp collisions the dependence on transverse momentum p_T of measured inclusive cross sections is generally well described by $d\sigma/dp_T^2 \propto e^{-bm_T}$, $m_T^2 = m^2 + p_T^2$ as illustrated in fig. 1.[5] An exponential shape is a simplified version of a thermodynamical distribution [6] similar to the classical Maxwell-Boltzmann distribution $d\sigma/dv^2 \propto e^{-E/kT}$, where v is a particle's velocity, E its energy, T a temperature. Hence the inverse slope 1/b ($\propto \langle p_T \rangle$) should be proportional to a temperature. Accepting this idea for the time being[7] one can think of the equivalent to a well-known experiment: heating of water. Measuring the temperature of water one finds first a rise, then a constant value of T while water undergoes a phase transition (of first order) to steam and finally the temperature of steam rises again. For pp collisions a similar pattern shows up: With increasing beam momentum p_B the value of $\langle p_T \rangle$ increases from $\langle p_T \rangle$ < 100 MeV/c at $p_B \leq 1$ GeV/c to a plateau with $\langle p_T \rangle \sim 330$ MeV/c at 70 GeV/c $\lesssim p_B \lesssim$ 2000 GeV/c. Are we therefore witnessing the onset of a phase transition, i.e., the "boiling" of hadronic matter [8] at the "Hagedorn" temperature T ~ 160 MeV?

2.2 Phase Transitions

There are simple arguments in favor of a phase transition to free quarks and gluons: Just as in the case of an insulator-conductor transition (e.g., gas → el.magn. plasma) one may expect sort of a Debye screening of color charges of quarks and gluons if collisions of heavy ions generate sufficiently dense matter. This is confirmed by recent QCD calculations on a lattice.[9a) The order of the phase transition is not yet firmly established.[9) Debye screening results in a small value of the strong coupling constant $\alpha_s(Q^2,T)$ [10) for large values of T and small values of a four-momentum transfer Q.

At a given beam momentum per nucleon N heavy ions should be more efficient than (anti-)protons in achieving a deconfining phase transition as a consequence of better screening and thermalization due to the larger numbers of quarks and gluons involved.

To get a more quantitative feeling of what may be needed to generate a phase transition experimentally, a gas of free, massless quarks and gluons is considered now. Masslessness ("chiral symmetry restoration") in the QGP is suggested by Lattice-QCD [11). It may be understood in analogy to electrons in a valence band of a conductor, where the effective electron mass differs from its vacuum value due to boundary conditions.

One easily calculates the energy density ε_q' (ε_g') per degree of freedom for free, massless quarks (gluons):

$$\varepsilon_q' = a \int dp \cdot p \cdot \mathrm{Bose}(T) = (\pi^2/30)\, T^4 \text{ and} \tag{1a}$$

$$\varepsilon_g' = a \int dp \cdot p \cdot \mathrm{Fermi}(T, \pm\mu). \tag{1b}$$

These relations correspond to the classical Stefan-Boltzmann law; Bose(T) and Fermi(T,±μ) stand for the Bose and Fermi distribution functions at given temperature T and chemical potential μ; normalization factors are contained in a. Multiplying by the number of degrees of freedom one gets an equation of state for the QGP, i.e., a relation between its energy density ε_Q, T and μ:

$$\varepsilon_Q = 2_s \cdot 8_C \cdot \varepsilon_g' + 2_s \cdot 3_C \cdot 2_F \cdot (\varepsilon_q' + \varepsilon_{\bar{q}}') = f(T,\mu). \qquad (2)$$

The subscripts symbolize color (C), flavor (F) and spin (s). The boundary $T_c(\mu_c)$ between hadronic phase (H) and QGP (Q) is obtained from the Gibbs relations for temperature, pressure (P) and chemical potential:

$$T_H = T_Q = T_c,\ P_H = P_Q = P_c,\ \mu_H = \mu_Q = \mu_c. \qquad (3)$$

A typical phase diagram is shown in fig. 2.[12)] Two extremes may occur: A QGP with $T \sim 0$ and large net baryon density n_B ($n_B \propto \mu_Q^3$) may exist in neutron stars and may be produced by stopping projectile nuclei by target nuclei with atomic masses B and A, respectively, at $p_B = 0(10\ \mathrm{GeV/c/N})$. The simpler case of a baryon free QGP ($\mu_Q = 0$) is evaluated in the following. It existed presumably during the early universe and may be produced in the central rapidity region of very high energy nuclear collisions. The integrals (1) are solved in this case analytically:

$$\varepsilon_Q(T,\mu_Q=0) = g_Q\ \pi^2/30\ T^4 \sim (T/160\ \mathrm{MeV})^4\ \mathrm{GeV/fm}^3; \qquad (4)$$

g_Q is the effective number of degrees of freedom. With $T_c(\mu_Q=0) =$ (200 ± 40) MeV from Lattice-QCD on arrives at $\epsilon_Q(T_c,\mu_Q=0) \sim 1\div5$ GeV/fm^3 with $\epsilon_Q\,(T_c,\mu_Q=0) \sim 2.5$ GeV/fm^3 as the most popular guess.

For comparison, the energy density ϵ_p of a proton is $\epsilon_p = m_p/V_p \sim$ 0.5 GeV/fm^3; for a nucleus A one finds $\epsilon_A = Am_A\ V_A \sim 0.16$ GeV/fm^3, while for an ultrarelativistic gas of free, massless, charged and neutral pions $\epsilon_\pi = 3\cdot(\pi^2/30)T^4 \sim T^4$. From these numbers one infers that energy densities about one order of magnitude larger than ϵ_π or ϵ_A have to be reached experimentally for a QGP to form. The latent heat $\epsilon_Q - \epsilon_H$ is needed for liberating the degrees of freedom in the QGP.

An interesting relation emerges from the equation $P_H = P_Q$ for $\mu=0$. Using the formula $P = 1/3\epsilon$ for relativistic gases as an approximation,[13] and taking into account the effect of vacuum pressure B (= bag constant), one arrives at $P_Q = 1/3\ (\epsilon_Q-3B) = 1/3\epsilon_\pi = P_H$. This yields then a remarkable, but simplified, correlation between quantities characterizing the QGP or the vacuum:

$$\frac{\pi^2}{90}(g_Q-3)T_c^4 = B. \qquad (5)$$

2.3 Space-Time History

The creation of a QGP, i.e. the transition from an ordered motion of incident partons to a thermalized behavior, is little understood. At $p_B \sim O(10$ GeV/c/N) this may be accomplished in compressed nuclear matter, created by stopping the projectile in the target nucleus. At very high energies, the Lorentz-contracted colliding nuclei are likely to exchange color such that the subsequent separation of color charges creates a strong color field[14] which, in turn, is a source of quark-antiquark pairs and gluons. This may lead to an equilibrated parton system with $n_B = 0$ and $T_i > T_c$ at a proper time τ_i. Bremsstrahlung gluon showers provide an alternative scenario at very high energies.[15] Heavy ion collisions at $p_B \sim O(100\ \mathrm{GeV/c/N})$ are presumably between those extremes.

It does not seem imperative for a QGP to form in every event or to occupy the whole interaction region, even if critical energy densities are reached.

At some point the dense matter thus created starts expanding and cooling. When the critical temperature T_c is reached at a time τ_Q, confinement sets in, potentially giving rise to a mixed phase. Once all partons are turned into primary hadrons at a time τ_M, further longitudinal collective expansion and cooling leads to a hadron density with a mean free path of the order of the size of the system. At this freeze-out density, hadrons escape freely with an energy distribution corresponding to the freeze-out temperature T_F, possibly Doppler-shifted due to transverse collective flow.

The space-time history for AA collisions at very high energy is given schematically in fig. 3.

Some instructive consequences of hydrodynamic flow are presented in the following. At very high energies one may assume that the particle density dN/dy_c is independent of center-of-mass rapidity y_c at $y_c \sim 0$, corresponding to invariance under longitudinal Lorentz-boosts. This leads initially to 1-dimensional "scaling" hydrodynamics of longitudinal expansion.[16] Assuming entropy conservation, i.e. absence of dissipative effects, hydrodynamic equations yield the relation $s \cdot \tau = \mathrm{const.}$, where the entropy density $s = dS/dV$ is obtained from the entropy S in a volume V, and τ is the proper time. The entropy per degree of freedom $c = dS/dn$ is a constant, $c = 3.6$ (4.2) for gluons (quarks). This yields the number dn of particles, $dn = \frac{1}{c}\, dV \cdot s$, within a cylindric volume element $dV = (dy_c \tau) \cdot \pi R_A^2$ for colliding nuclei with radii $R_A \propto A^{1/3}$. Thus, one arrives at

$$\frac{dn}{dy_c} = \frac{1}{c}\, \pi R_A^2\, \tau . s = \text{const.} \tag{6}$$

From equ. (6) one can therefore determine the initial density of partons from the measured density of hadrons. Using, finally, the thermodynamic relation $s \propto \frac{\partial \varepsilon}{\partial T} \propto T^3$ and $\frac{dn}{dy} \propto A^1$, which is compatible with cosmic ray events,[17] one ends up with $s \cdot \tau \propto \tau_i T_i^3 \propto A^{1/3}$. One possible solution[18] is $\tau_i \propto A^{-1/6}$ and $T_i \propto A^{1/6}$. This underlines the usefulness of heavy nuclei in achieving high QGP temperatures in a short period of time.

Based on the relation $s \cdot \tau$ = const. one can furthermore estimate the times τ_Q, τ_M, τ_F, when the QGP, the mixed phase and the interacting hadron gas, respectively, cease to exist:

$$\tau_Q = \tau_i \left(\frac{T_i}{T_c}\right)^3 = A^{1/3}, \quad \tau_M = \tau_Q \left(\frac{S_Q}{S_H}\right) = \tau_Q \left(\frac{g_Q}{g_H}\right) \sim \tau_Q \cdot 10 \text{ and } \tau_F = \tau_M \left(\frac{T_c}{T_F}\right)^3. \tag{7}$$

One sees readily, that τ_Q is larger for heavier nuclei, and that much more time is spent in the mixed phase at T_c than in the deconfined phase with $T_i > T_c$. Hence the mixed phase may be more easily accessible in an experiment.

3. EXPERIMENTS

One usually attempts to meet the condition of high energy densities by triggering on events where projectile (B) and target (A) collide head on ("central collisions") as illustrated in fig. 4; this is signaled by the absence of projectile nucleons at small polar lab angles θ. As a consequence, many experiments exhibit the common feature of hadronic calorimetry at $\theta \sim 0°$. A fraction of the projectile energy is transformed into transverse energy E_T. This transverse energy flow is, in most experiments, detected by el.magn. and hadronic calorimeters. The experiments differ, on the other hand, in that various specialized detectors are used to search for different signatures of the QGP.

The Plastic Ball of WA80 covers the lab pseudorapidity range $-1.7 \leq \eta \leq 1.3$ (fig. 5). Its 655 ΔE-E modules identify nuclei up to He for a detailed study of target fragmentation. Photons at $1.5 \leq \eta \leq 2.1$ are detected by a Pb-glass array.

Experiment NA38 employs a well-proven spectrometer (fig. 6) to study production of μ-pairs with masses $M_{\mu\mu} > 0.5$ GeV at $2.8 \leq \eta \leq 4$. In this experiment, the beam hits 10 subtargets sequentially; scintillation counters determine the target which had caused the interaction.

In addition to a μ-pair spectrometer, NA34 uses an external spectrometer arm to identify particles and photons at $0.9 \leq \eta \leq 2$ which fits into a slit of their 4π calorimeter (fig. 7). Charged multiplicities for $0.9 \leq \eta \leq 5$ are derived from highly segmented silicon detectors.

The essential component of BNL experiment E802 (fig. 8) is a dedicated single-arm spectrometer for hadron identification in the range $0.7 \leq \eta \leq 3.1$.

While the flux of charged kaons can be measured by NA34 and E802, experiments WA85, NA35 and NA36 focus on the detection of the neutral strange particles K_S^0 and $\overset{(-)}{\Lambda}$.

Experiment WA85 modified the Ω' spectrometer (fig. 9) by reducing the sensitive area of its multi-wire proportional chambers to a "butterfly" shape. Hence, only about 1.7 tracks per event with $p_T > 0.6$ GeV/c are detected in the range $2.2 \leq \eta \leq 3.2$. Silicon microstrip counters yield information on the charged multiplicity for $2.1 \leq \eta \leq 3.4$.

A streamer chamber allows NA35 (fig. 10) to visually inspect nearly complete events, especially tracks with lab rapidities y in the range $0.45 \leq y \leq 4.55$.

The TPC of NA36 (fig. 11) is placed above the beam and covers the range $y > 2.5$. It provides 3-dimensional tracking and is read out digitally. The high charged multiplicities in central S-Pb collisions at 200 GeV/c/N are routinely reconstructed. Sufficient statistics for a first look at rare processes such as Ξ or Ω production should be within reach.

There is also a number of emulsion experiments. This technique yields the most accurate information on tracking of charged particles. It is therefore a very essential and reliable source of information, particularly on processes with moderate or large cross sections.

4. Global Features of Nuclear Interactions

4.1 Cross Sections

The most fundamental quantity characterizing an interaction is the total cross section. Due to many possible types of processes in nuclear collisions and to related experimental difficulties, two partial cross sections are of more practical value: 1), the charge changing cross section $\sigma_{\Delta Z}$ which measures all processes in which at least one proton is removed from the projectile, 2) the reaction cross section σ_R which includes pure nuclear fragmentation (σ_F) and inelastic processes (σ_{in}) transforming kinetic energy into secondary particles. Data at lower energies are consistent with the relation $\sigma_{\Delta Z} \leq \sigma_R \sim \sigma_F + \sigma_{in}$, since σ_R receives also contributions from neutron "removal" processes.

The measured cross sections $\sigma_{\Delta Z}$ for oxygen-nucleus collisions[19] at 60 and 200 GeV/c/N turned out to be much larger than i) corresponding inelastic cross sections at the same energies[20] and ii) reaction cross sections determined at beam momenta $p_B \leq 4.5$ GeV/c/N.[21] To clarify the situation, both σ_{in} and $\sigma_{\Delta Z}$ were recently determined for sulphur beams at 200 GeV/c/N by NA36;[22] the square roots of these cross sections are shown in fig. 12. At all energies, the data are now compatible with σ_{in} ($\sim \sigma_R$) $\propto \pi R^2$, where $R = R_A + R_B - \delta$ contains the sum of the nuclear radii $R_I = r_o I^{1/3}$ with $I = A,B$, and $r_o \sim 1.2$ fm, $\delta \sim 1.32$.

The difference between $\sigma_{\Delta Z}$ (fig. 12a) and σ_{in} (fig. 12b) increases from about 0.1b for Al targets to about 3b for Pb targets. This is compatible with a power law as expected from el.magn. dissociation (ED):[23] The charges of the ions passing each other at high velocity and large impact parameter $b > R_A + R_B$, where strong interactions are negligible, generate extremely strong el.magn. fields of short duration. Thereby multipole resonances are excited, e.g., in the projectile, which decay via emission of neutrons or protons. Being of electromagnetic origin, the corresponding cross section σ_{ED} should be proportional to the square of an effective target charge Z_{eff}, i.e. $\sigma_{ED} \propto Z^2_{eff}$, where $Z_{eff} \sim A/2$. Quantitative theoretical predictions are obtained in the framework of one-photon exchange using experimental data on photonuclear cross sections.[23)]

In fig. 13 the calculated cross sections σ_{ED} ($O\,{}^{197}Au \rightarrow {}^{196}Au + X$) for el.magn. target dissociation are about 30% larger than the cross sections measured by NA40,[24)] which are on the level of about $0.1\sigma_{in}$.

For colliding gold beams of 100 GeV/c/N, $\sigma_{ED} \sim 60b \sim 10\sigma_{in}$ has been predicted.[24)] While el.magn. processes limit beam lifetimes in high energy ion colliders and are therefore of some concern, they are also useful potential sources of exotic nuclei.[25a)] It is furthermore speculated that collisions of heavy ions yield substantial numbers of "$\gamma\gamma$" events[25b)] in which two virtual γ, one coupled to each ion, create a pair of charged fermions.

4.2 Nuclear Projectile Fragmentation and Forward Energy Flow

Nuclear fragmentation[26,27)] influences directly the design of experiments. The angular distribution of projectile fragments must be known to optimize the measurement of baryonic energy flow at small polar lab angles θ. This flow is proportional to the number of non-interacting ("spectator") nucleons. It is presumably governed by the geometry of a collision and tends to vanish for central collisions, if $B \leq A$, as shown in fig. 4.

A measurement by emulsion experiment EMU1[28)] of the distribution of projected polar angles $\theta_{x,y}$ for He fragments from an oxygen beam at 200 GeV/c/N is displayed in fig. 14. The dispersion $\sigma_{\theta_x} = 20 \cdot 10^{-2}$ mrad of the Gaussian distribution can be reproduced assuming that the Fermi momenta of 4 nucleons combine randomly.[29] Most fragments are contained in the angular range $\theta \leq 3 \cdot \sqrt{2} \cdot \sigma_{\theta_x} \sim 0.1°(0.35°)$ at 200 (60) GeV/c/N.

Forward energy flow was recorded by NA35, NA36 and WA80 for $\theta \lesssim 0.4°$. Spectra from the latter experiment are shown in fig. 15 for oxygen beams at 60 and 200 GeV/c/N and various targets.[30] As one increases the target size one finds more and more "central" events where the projectile nucleus has dissipated most of its incident lab momentum. This is more pronounced at p_B = 60 GeV/c/N. From these measurements one concludes that light targets do not efficiently stop the projectile nuclei. This is to a large extent a direct consequence of geometry, since two equal-sized objects do not completely overlap frequently. At 200 GeV/c/N the spectra are rather well reproduced by the Fritjof Monte Carlo code.[31] Crucial ingredients are the shape and size of the colliding nuclei determining the number of independent NN collisions, as well as the assumption of straight line trajectories of the incident nucleons in the spirit of Glauber theory.[32] The forward energy flow should therefore be proportional to the number of projectile spectator nucleons such that it provides a good trigger on collision geometry. Strictly speaking, this can only be true, if a contribution from secondary particles were negligible; this is less obvious for central collisions. A measurement of forward energy flow may be affected by other nearby detectors which may generate particle showers in secondary interactions. This renders a quantitative comparison between different experiments rather cumbersome. The energy flow at $\theta \lesssim 0.3°$ in fig. 16, recently obtained by NA36[33] from a sulfur beam at 200 GeV/c/N, exhibits trends similar to those from oxygen beams (fig. 15).

These measurements prove that one can deposit a large amount of energy in the volume of the interaction with a sufficient cross section. Thus final states emerge with a large number of mesons and/or with large energies per meson.

4.3 Multiplicity Distributions

An unbiased distribution of the multiplicity n_s of minimum ionizing ("shower") particles, i.e., $\psi(z) = \langle n_s \rangle \sigma_{n_s}/\sigma_{in}$, $z = n_s/\langle n_s \rangle$, was obtained by emulsion experiment EMU5[34] from oxygen collisions at 200 GeV/c/N with a lead target; it is shown in fig. 17. A maximum is found at $z \lesssim 0.2$, followed by a plateau and a further decrease. The measurement is compatible with data from the cosmic ray experiment JACEE[34] and from the emulsion experiment EMU3 using oxygen beams at 60 GeV/c/N.[35] The wide distribution in fig. 17 differs significantly from the well known KNO shape for pp collisions, but is well described by a calculation in the framework of the Dual-Parton model extended to nucleus-nucleus collisions;[36] an average number $\langle n_- \rangle \sim 40$ of negative particles is predicted, while $\langle n_s \rangle \sim 2\langle n_- \rangle = 88$ was measured.[34] Scaled multiplicity distributions for negative particles (mainly π^-) produced by oxygen beams at 60 and 200 GeV/c/N on Cu and Au targets were also obtained by NA35:[20] No dependence either on cms energy or on target mass is found (fig. 17b,c) suggesting a dominating role of collision geometry. For central O-Au collisions (at 200 GeV/c/N) selected on the basis of forward energy flow, a very narrow distribution in z is obtained[20] with an average charged multiplicity $<n_c>_{central} \sim 286$, i.e. $<z> = n_c/<n_c> \gtrsim 3$, and a dispersion $D \sim 50$. The small value of D results from the suppression of non-central collisions with impact parameters $b > 0$. Hence all projectile nucleons interact in this case. It is then straight-forward to assume that, for decreasing z, less projectile nucleons are involved. Events with $z \lesssim 0.2$ should then be due to rather abundant peripheral collisions with a large forward energy flow. Such a geometrical picture is supported qualitatively by emulsion data from EMU1,[28] where a linear increase of $<n_s>$ as function of the number of interacting projectile protons was measured (fig. 18).

As mentioned above, experiments have to deal with about 280 charged secondaries in central O-Au collisions at 200 GeV/c/N; for central events from sulfur and lead collisions with lead targets at the same energy one expects then about 560 and up to 3500 charged mesons. A comparison with $<n_c> \sim 8$ for pp collisions at the same beam momentum underlines the experimental challenge. A positive consequence of this wealth of information is that a rather complete characterization of the dynamics of individual events might become feasible (see section 4.6).

4.4 Rapidity Distributions

In the geometric framework, the dependence of the velocity in the lab of the rest system of the participating nucleons (cms) on forward energy flow is calculable. This is of practical importance since detector acceptances are usually fixed in the lab system. For peripheral events, the cms coincides with the nucleon-nucleon rest system. In central events all B (<A) projectile

nucleons interact with P_A target nucleons occupying a cylinder of radius $r_0 B^{1/3}$ through the center of the target. The lab rapidity $y(B+P_A)$ of this asymmetric system of nucleons is then given by the lab rapidity y_0 of a symmetric system (e.g. of pp collisions) minus a correction term:[37)] $y(B+P_A) = y_0 - 1/2 \ln (^{P_A}/_B)$. Corrected lab (pseudo-)rapidity distributions are displayed in fig. 19 for negative particles from central O-Au collisions[38)] (NA35) and in fig. 20 for shower particles from central O-AgBr interactions.[28,39)] Maxima are found at a (pseudo-)rapidity of about 2.45 as expected from the formula above ($B = 16$, $P_A \sim 55$), whereas distributions from pp collisions are centered at $y = 3.0$.

The emulsion data in fig. 20 are well reproduced by Fritjof predictions down to target rapidities. This is rather surprising since cascading of hadrons inside the target is not included in the model. There is no strong evidence for cascading from negative particle production at $y \lesssim 2$ in fig. 19, either, when compared to the substantial yields at $y < 2$ of shower and negative particles measured in pAu and pXe collisions at 200 GeV/c, respectively.[40)] The apparent absence of cascading for nuclear beams may be related to the strong increase of the number of protons and neutrons at $\eta \lesssim 1$ in oxygen induced central reactions relative to p beams as measured by WA80[41)] (fig. 21). It suggests that the target breaks up completely into single nucleons which also experience substantial acceleration; hence the picture of "spectators" breaks down. Such a dilute system of target nucleons does not favor cascading. Target disintegration may also explain partially the discrepancy between predicted and measured pseudorapidity distributions which is found by WA80[41)] for charged secondaries at $\eta < 3$.

Comparisons of the average rapidity with a prediction from collision geometry, and of the widths Δy_{FWHM} with results from pp interactions (see below) are, of course, only meaningful, if there is no strong cascading.

The width of the distribution in fig. 19, $\Delta y_{FWHM} \sim 3.1$ at 200 GeV/c/N, is smaller than $\Delta y_{FWHM} \sim 4.0$ measured for inclusive production of negative particles in pp collisions at the same beam momentum.[43a] In pp collisions, the width decreases with increasing scaled charged multiplicity $n_c/\sqrt{s}$,[43b] such that $\Delta y_{FWHM} \sim 3.0$ would correspond to $z = n_c/\langle n_c \rangle \sim 2$ at 200 GeV/c. Isotropic emission of pions would correspond to $\Delta y_{FWHM} \sim 1.8$ for temperatures $T > 100$ MeV.[38]

Searches for non-statistical fluctuations of dn/dy are in progress.[28] Fluctuations are expected e.g. from a formation of plasma droplets.[44] Non-statistical fluctuations may have been seen in cosmic ray events,[34] as well as in pp collisions.[45]

4.5 Transverse Energy and Energy Density

If the energy per pion E_π did not vary substantially with the "centrality" of a collision one expected similar shapes for the distributions dN/dn_c and $d\sigma/dE_T$; here $E_T \propto n_c \cdot E_\pi$ denotes transverse energy.

Transverse energy distributions from E802[46,47] and NA35[48] for O-Au collisions at various beam momenta are compiled[49] in fig. 22; the data at p_B = 14.5 GeV/c/N (E802) were slightly scaled[49] in order to correspond to a common interval Δy. Obviously, the shapes of these spectra closely resemble the one of the multiplicity distributions (fig. 17). As in the latter case, the distributions can be thought of as up to 16-fold convolutions of spectra from pAu collisions.[46,50] The end of the plateau corresponds to central collisions with 16 participating projectile nucleons.

The significance of the energy dependence observed in fig. 22 is understood in the following way: The maximal transverse energy E_{Tmax} created by isotropic emission of the energy $E_{max} = \sqrt{s}(B+P_A) - (B+P_A) \cdot m_N$ available for production of particles in central collisions is given by $E_{Tmax} = \frac{\pi}{4} E_{max}$. The invariant energy $\sqrt{s}(B+P_A)$ is calculated from all B projectile nucleons and P_A target participants; P_A is fixed by the geometry of central collisions, and m_N is the nucleon mass. With E_T^F denoting the value of E_T for a fixed cross section outside the plateau, one finds that the ratio E_T^F/E_{Tmax} decreases at higher beam momenta. This suggests that lower beam energies are more efficiently converted into transverse energy. It should, however, be noted that the assumption of isotropic emission is not borne out by the data (see section 4.4) obtained at 60 and 200 GeV/c/N. Evidence for near isotropy was, on the other hand, obtained by E814 from Si-A collisions at 10 GeV/c/N.[51]

The dependence on target mass of E_T spectra in the interval $2.28 \leq y \leq 3.94$ can be derived from measurements by NA35[48] presented as function of $x = E_T/E_{Tmax}$ in fig. 23. For $x \gtrsim 0.4$ the distributions tend to scale in x. This means that the transverse energy at fixed cross section, E_T^F, is proportional to $E_{Tmax} \propto A^{\alpha}$, with $\alpha \sim 0.2$.[48]

For the pseudorapidity range $-0.1 \leq \eta \leq 2.9$ NA34 has measured cross sections as function of E_T for oxygen[52] and sulfur[53] beams (fig. 24,25). Several interesting features emerge:

i. The spectra from oxygen and sulfur beams incident on, e.g., tungsten targets would coincide if the E_T scale were expanded by a factor $f \sim 1.55$ for oxygen projectiles. For gold targets NA35[48] (WA80[54]) finds $f \sim 1.8$ (1.65). These values of f are close to the ratios $E_{max}(S)/E_{max}(0) \sim 1.8$, and to the ratio of cross sections of the projectiles, i.e. to $(R_S/R_O)^2 \sim 1.6$. The naive scheme of B-fold convolutions of spectra from pA collisions[46,50] would yield $f = 2$.

ii. A remarkable demonstration of the dominating role of collision geometry is provided by the substantial difference of cross sections at given E_T for Pb and U targets in fig. 25: It is a consequence of the rather large quadrupole moment of uranium.

iii. The oxygen data in fig. 24 are generally well reproduced by the Dual-Parton model,[53] which, however, yields smaller cross sections for very large transverse energies. This may either be attributed partially to the systematic uncertainty (7%) of the E_T scale, or to potential cascading processes.[55] On the other hand, a comparison of the differential cross sections $d^2\sigma/dE_T dy$ for pPb and OPb collisions in figs. 26[56] and 27[52] tends to support much stronger cascading at $\eta < 1.8$ and at large E_T for pPb collisions. As discussed in section 4.4, the rapidity distributions from shower or negative particles do not show any obvious cascading effect for central O-A collisions. A better understanding of reinteraction processes is obviously needed.

To estimate typical energy densities ε from E_T measurements in central collisions one may proceed as follows: For a system of $(B + P_A)$ nucleons with total energy E_{max} decaying isotropically ("fireball") one finds $dE_T/dy \sim E_{max}/2$. Consequently, the energy density $\varepsilon_F = E_{max}/V = 2 \cdot dE_T/dy/V$ can be calculated from the Lorentz-contracted volume V occupied by $B + P_A$ nucleons, $V = \pi r_o^3 B^{2/3} A^{1/3}/\gamma$. For a central O-Au collision at 200 GeV/c/N with $E_T \sim 120$ GeV (fig. 22) one obtains $\varepsilon_F \sim 4$ GeV/fm^3.

With the Bjorken formula[16] $\varepsilon_B = \frac{dE_T}{dy}/(\pi R_B^2 \tau)$, which is equivalent to equ. (6), one arrives at $\varepsilon_B \sim 3$ GeV/fm^3 for $\tau = 1$ fm/c.

While it is encouraging to discover that these experimental estimates are close to the predicted critical density $\varepsilon_Q \sim 2.5$ GeV/fm^3 (section 2.2), it should be stressed that none of the assumptions involved in the calculations was verified experimentally; in addition the value of τ is rather uncertain.[57]

Based on the formulae for ε_F and ε_B, and from the measured dependence of dE_T/dy on the masses of the colliding nuclei, one does not expect a strong increase of energy density with the masses of interacting nuclei. On the other hand, both dE_T/dy and the Lorentz-factor γ are roughly proportional to $\sqrt{s}(B + P_A)$, such that significantly higher energy densities are expected at higher beam momenta.

Heavier nuclei are nevertheless preferable, since they are expected to lead to more efficient thermalization, higher initial temperatures and therefore to a longer duration of the Quark-Gluon plasma and of the mixed phase (section 2.3).

4.6 Boson Interferometry

The space-time history of the interaction region can be investigated experimentally by measurements of Bose-Einstein interferometry. Borrowed from astronomy,[58] this has become a well-established tool in high energy reactions.[59] The normalized interference pattern $C(q_1, q_2) = P(q_1, q_2)/P(q_1)P(q_2)$ of pairs of identical bosons originating from a chaotic source corresponds to the Fourier-transformed intensity distribution of the source at the time the detected bosons were emitted; $P(q_i)$ $(P(q_1 \cdot q_2))$ is the probability to observe (a pair of) bosons with four-momenta q_i, $i = 1,2$. The product $P(q_1) \cdot P(q_2)$ corresponds to uncorrelated production; it is usually determined by combining particles from different events, such that acceptance effects are minimized when determining $C(q_1, q_2)$.

A very popular parameterization of the interference pattern is given by $C(q_1, q_2) = A[1 + \lambda \exp(-Q_T^2 R_T^2/2)\exp(-Q_L^2 R_L^2/2)]$. In this approximation Q_T (Q_L) is the projection of the difference of three-momenta $\vec{Q} = \vec{q}_1 - \vec{q}_2$, perpendicular (parallel) to the beam direction. The distributions of Q_T and Q_L reflect the spatial dimensions R_T and R_L of the source in a Lorentz-non-invariant way; a potential time dependence is integrated over. The factor A is a normalization constant and $\lambda = 1(0)$ for a completely chaotic (coherent) source of identified bosons.

Fits of this parametrization to Gamov-corrected correlation functions from pairs of negative particles are shown in fig. 28 for various intervals of y. The analysis is based upon about $2 \cdot 10^5$ pairs of negative particles from 105 central O-Au events measured with the NA35 streamer chamber.[60] At $Q_T < 100$ MeV/c one finds a sharp correlation pattern with $C\ (Q_T = 0) \sim 1.2 \div 1.4$.

A formulation of the correlation function incorporating longitudinal expansion is due to Kolehmainen and Gyulassy.[61] Once the temperature of the source is fixed, e.g. on the basis of measured average transverse momenta (see section 5.1), the free parameters are R_T, the proper freeze-out time τ_0, and the chaoticity parameter λ. These parameters were determined from a fit and are given as a function of y in fig. 29.[60] The measured values of all parameters tend to increase by about a factor 2 ÷ 3 between $y < 2$ and $\langle y \rangle \sim 2.5$; the significance is about 2 standard deviations from only 105 central events. The most straightforward interpretation of this observation is that, for $y < 2$, pions are emitted from a rather coherent source with the transverse dimension of oxygen; the freeze-out time is about equal to the time oxygen needs to traverse the Au target. This leaves little room for expansion and thermalization. Central pairs with $2 \leq y \leq 3$, on the other hand, tend to be created in a rather large volume with $R_T \sim 7$ fm, at $\tau_0 = 6.4$ fm/c, which is probably a sufficiently long time for thermalization. This would correspond to a large value of λ, and is consistent with the data. Before claiming evidence for collective expansion to a state of relatively low energy density the influence of resonances has to be resolved.[62] This first investigation of Bose-Einstein correlations proves the potential of providing detailed information on dynamics. Measurements even of single events become feasible for heavy nuclei.[60] For fixed target experiments with heavy ions at high energy one has to cope with challenging experimental problems: The half-width of the interference pattern is proportional to $1/R_T$. For Pb-Pb collisions one must therefore measure momentum differences $Q_T << 40$ MeV/c with sufficient precision. In streamer chamber experiments one faces the difficulty of matching very close tracks from 2 different 2-dimensional projections of an event. Therefore 3-dimensional tracking, such as in a TPC, is called for.

A full exploitation of interferometry combined with good statistics, precise tracking and reliable particle identification may help to verify the existence of the QGP[62,63] in the future.

5. Search for the QGP

5.1 Transverse momenta

Measured cross sections $d\sigma/dp_T^2$ for inclusive production of secondaries in pp collisions are usually consistent with thermal distributions with $T > 135$ MeV, as illustrated in fig. 1. Collective flow in nuclear collisions would modify these spectra.[64] The flow velocity is a function of time and related to the temperature at this time. Hence, the two factors determining the shape of $d\sigma/dp_T^2$, i.e. temperature and flow, may not be separable easily in a model-insensitive way. A way out is to measure these cross sections separately for identified particles, since a common flow velocity affects the momenta of heavier particles more strongly.[64]

The p_T distribution for negative particles with $2 < y < 3$ in fig. 30a, obtained by NA35 from central O-Au collisions,[38] is significantly different from those presented in fig. 1; there is a clear change of slope at $p_T \sim$ 0.3 GeV/c as in the case of p-Au collisions (not shown). A good fit with two thermal sources yields the temperatures $T_1 = 43$ MeV and $T_2 = 153$ MeV. One concludes therefore, that the data at $p_T < 0.3$ MeV/c correspond to a lower temperature than the one extracted from pp collisions.[38] In case of collective expansion in nuclear collisions (see section 4.6), hadrons would decouple from a hadron gas of low energy density ε, corresponding to low temperatures $T \sim \sqrt[4]{\varepsilon}$; this is qualitatively consistent with the observed p_T spectra.

For negative particles at $p_T < 0.25$ GeV/c strong enhancements were also observed at 200 GeV/c/N by NA34 in both central O-Au collisions and pW interactions with $E_T > 10$ GeV,[65] as well as for shower particles from central collisions of cosmic rays ($p_B \sim 10 \div 250$ GeV/c/N) with emulsion nuclei (Ag/Br).[66] The latter data are well reproduced assuming an emitting source of temperature $T = \langle p_T \rangle / 2\gamma = 78$ MeV expanding with $\beta = 0.61$. Differences between the measurements in refs 65,66 and 43 for $p_T \lesssim 0.15$ GeV/c may be (partially) due to different contributions of electrons from γ conversion and Dalitz decays of π°. A potentially large effect is implied by pp data.[67]. All available data including those on π° production by WA80[68] in fig. 30b tend to be consistent for $p_T > 0.4$ GeV/c.

Based upon the trends emerging from p_T spectra and from pion interferometry it was concluded[69] that collective effects are established in ion collisions and, consequently, that the picture of independent nucleon-nucleon interactions is insufficient.

While this may still be true, the excess of particles with $p_T < 0.25$ GeV/c relative to the inclusive yields in high multiplicity ($z > 1.5$) events from pp and $\alpha\alpha$ collisions should be pointed out.[70,71] A more careful evaluation of similarities and possible interpretations of data from pp collisions is mandatory before safe conclusions can be drawn. The lesson to be learned is that one must gain an understanding of pp, pA and BA collisions on the same level of detail to unveil the secrets of the QGP.

The yields per nucleon of secondaries with $p_T \gtrsim 1$ GeV/c in oxygen induced reactions[38,65,68] are larger than in pp collisions as shown for π^0 in fig. 30b.[68]. This is an established fact for pA collisions, where this "Cronin" effect[72] can be explained by hard multiple scattering[73] of incident partons in the target nucleus. For BA collisions one expects therefore similar trends and interpretations.

The dependence of $d\sigma/dp_T^2$ on dn/dy ~ s (section 2.3) is predicted[64] to reflect rather directly the occurrence of a phase transition of first order to a QGP. It is sufficient to consider here the first moment, $\langle p_T \rangle$, of the distribution. For a given phase of strongly interacting matter -- hadron gas or QGP -- one has the relations $\langle p_T \rangle \propto T$ and $dn/dy \propto s \propto \frac{\partial \varepsilon}{\partial T} \propto T^3$, whence a rather linear dependence of $\langle p_T \rangle$ on ln(dn/dy). This is illustrated for a pion gas in fig. 31.[64] At the phase transition to the QGP, temperature stays constant at $T = T_c$, i.e. $\langle p_T \rangle$ does not change, while an increase of entropy liberates the larger number of degrees of freedom of free quarks and gluons. A further increase of $\langle p_T \rangle$ at $T > T_c$ originates from collective transverse flow in the QGP. At fixed $dn/dy \propto s$ one expects larger transverse momenta $\langle p_T \rangle \propto T$ in the hadron phase, since the smaller number of degrees of freedom must be compensated by a larger temperature T (fig. 31).

Correlations between the average momenta of pions and multiplicities have been studied experimentally. No significant variation of $\langle p_T \rangle$ with n_c or E_T was found so far, neither for pA[40b] nor for BA[38,74,68] collisions at 60 and 200 GeV/c/N. Typical data obtained by NA34[74] for negative particles ($0.5 \leq p_T \leq 2$ GeV/c) from p, O and S beams are shown in fig. 32, where a determination of dn/dy was replaced by a measurement of E_T. It is worth pointing out that observable effects are expected for $\frac{1}{A}\frac{dn}{dy} > 10$ (fig. 31), a range of densities not yet accessible in present experiments.

Data on this type of correlations from $\overset{(-)}{p}p$, dd, and $\alpha\alpha$ interactions reveal complex dependences on $\sqrt{s}$ and on the range of rapidity studied,[75,76,77] such that detailed analyses of identified particles from ion collisions seem to be required to reach reliable conclusions. The very high values of $\langle p_T \rangle$ derived by the JACEE collaboration[34] from very high energy cosmic ray interactions continue to resist a simple explanation.

5.2 Real and Virtual Photons

The most reliable messengers carrying information from the interior of the interaction volume are probes without strong interactions. Such probes are real photons or virtual photons (lepton-antilepton pairs, $\ell\bar{\ell}$). They are mainly created by the processes $qg \rightarrow q\gamma$ and $\bar{q}q \rightarrow \gamma^* \rightarrow \ell\bar{\ell}$. The production rate is proportional to T^4 (Stefan-Boltzmann law), hence it is sensitive to the largest temperature attained in a collision. As T is proportional to the average energy of equilibrated partons, the energies of the emerging (virtual) photons are related to the temperature at emission; this defines roughly the range of momenta (masses) of the photons (lepton pairs) of interest. As the partons involved are subject to collective flow, also the spectra of real or virtual photons are affected by it.[78] A direct consequence of scaling hydrodynamics (i.e. equ. (6)) is the proportionality between the average number of (virtual) photons and the square of the hadron density dn/dy.[79] This is common to all processes which are not due to the ordered, incoming partons. Indications for such a proportionality were found for lepton production in pp collisions.[80]

Any measurement of (virtual) photons is hampered by substantial background sources, such as meson decays into photons and lepton pairs. Real photons may be faked by misidentified charged hadrons and (anti-) neutrons. Potential backgrounds to the expected yield of dileptons from the QGP may come also from annihilation processes in a hadron gas at $T < T_c$, semileptonic decays of pairs of charmed mesons[81] and the Drell-Yan process.[82]

Pion annihilation may have shown up in recent data on dilepton production in pBe collisions at $p_B = 4.9$ GeV/c.[83]

So far, no firm data on production of non-resonant dileptons are available, while there is a first indication for a rather large yield of single photons at $p_T > 3$ GeV/c.[84]

5.3 Strange and charm quarks

It seems plausible to assume that heavy flavored quarks are good penetrating probes with an abundance related to temperature.[85] The argument for strange quarks goes basically as follows: At a given temperature the ratio of relative densities of strange quarks $\overset{(-)}{s}$ and light quarks $\overset{(-)}{q}$ and of kaons and pions from a QGP and a hadron gas, respectively, is given by the ratio of Boltzmann factors $e^{-(m_s - m_q)/T}/(e^{-(m_K - m_\pi)/T})$; since $(m_s - m_q) < (m_K - m_\pi)$ one finds a temperature dependent enhancement of strangeness in the QGP relative to the hadron phase. In baryon rich plasmas strange quarks would, in addition, be less suppressed by Pauli blocking than the much more abundant light quarks.

Once created in the QGP, strange quarks survive all further strong interactions due to strangeness conservation, and since $\bar{s}s$ annihilation is in general negligible.

Experimentally, however, one detects strange hadrons, which are created in a quark confining transition. This is in marked contrast to the electromagnetic probes. The hadronization process of quarks and gluons from a QGP is not well established; it may proceed, for example, by quark-antiquark recombination into mesons (e.g. $q\bar{q} \rightarrow \pi^0$) similar to a chemical reaction.[85] Since each degree of freedom corresponds to a fixed entropy, entropy would decrease in recombination processes. This problem may be avoided by considering recombination of quark-antiquark pairs into mesons of higher spin, or by the creation of $q\bar{q}$ pairs by string fragmentation as in e^+e^- annihilation.[86]

There are further intricate questions concerning e.g. chemical equilibrium in the QGP, inelastic hadronic interactions in and equilibration of the hadron gas.

It is therefore not trivial to assume that final yields of strange hadrons are strongly correlated with the abundance of strange quarks in the QGP, and a quantitative prediction is very involved.[85,87] One would, however, expect that the production rates of (anti-)cascades and (anti-)omegas which contain 2 or 3 $\overset{(-)}{s}$-quarks are more sensitive to the $\overset{(-)}{s}$-quark density in the QGP than the ones of kaons and lambdas.

Solid data are obviously needed in order to improve on existing theoretical models. Preliminary results by E802 on the inclusive ratios of charged kaons and pions in Si-Au collisions at p_B = 14.5 GeV/c/N reveal a very promising trend.[88] Employing a time-of flight array with an excellent time resolution an inclusive ratio $\frac{K^+}{\pi^+} \sim 0.2$ was measured in the range $1.4 \leq \eta \leq 2.1$. This is larger than the corresponding ratio in pp collisions, while the ratio $\frac{K^-}{\pi^-}$ (~0.05) was found to be consistent with results from pp collisions. From hadronization of a baryon rich QGP one expects naively larger yields of $K^+(u\bar{s})$ than of $K^-(\bar{u}s)$, since u-quarks are more abundant than $\bar{u}$-quarks. However, it was pointed out,[89] that inelastic reactions in the hadron gas tend to lead to a similar result. In passing it should be mentioned that also the very large yield of Λ in $\bar{p}$Ta interactions at 4 GeV/c[90] is so far compatible both with an interpretation in the framework of QGP formation[91] and in terms of inelastic reactions in dense hadronic matter.[90]

In central O-Au collisions at 60 and 200 GeV/c/N production of K^0_S, Λ and $\bar{\Lambda}$ is being investigated by NA35[92] for $p_T > 0.6$ GeV/c and $1.4 \leq y \leq 3.0$. The kinematic cuts were imposed to obtain clean signals in a high multiplicity environment. The measured inclusive strange particle yields relative to the inclusive flux of π^- are the same for O-Au and p-Au collisions. The Fritjof Monte Carlo code reproduces so far only inclusive cross sections for $K^\circ_S = \frac{1}{2}(K^\circ + \bar{K}^\circ)$ and π^- production.

A first analysis by WA85[93] of $\bar{\Lambda}$ and Λ production in S-W collisions yields clear signals, as shown in fig. 33 (shaded area) for (anti-) lambdas with $p_T > 0.6$ GeV/c. The reconstructed decay vertex is required to be far from the target to disfavor random combinations. Nearly all reconstructed (anti-) proton-pion systems with invariant masses bigger than about 1.4 GeV are easily removed by requiring that the respective tracks do come directly from the target.

A TPC was built by NA36 to measure particle trajectories in 3 dimensions.

The aim of the experiment is to investigate inclusive production of strange particles, including multistrange (anti-)baryons, for $p_T > 0.3$ GeV/c. A reconstructed event obtained from a sulphur beam is displayed in fig. 34.[94] This event happens to contain a decay of a neutral particle, probably of a lambda, which is easily reconstructed due to rather simple pattern recognition in three dimensions. Up to about 150 tracks per S-Pb collision have been found so far in the rather small ($50 \cdot 50 \cdot 100$ cm^3) TPC; this is about 5 times larger than the average charged multiplicity $\langle n_C \rangle$ from $p\bar{p}$ collisions at $\sqrt{s} = 540$ GeV.

More and better data on yields of strange hadrons are needed and expected for the near future.

Formation of strange matter[95] is another interesting facet of the QGP: The enhanced "evaporation" of K^+ discussed above leads to a QGP with net strangeness, which may subsequently turn into baryonic matter with a large fraction of s-quarks. This type of matter may be stable; its experimental signature is supposedly a rather small charge-to-mass ratio. No experiment is focused on strange matter so far, which would be a rather unique but probably rare signature of the QGP.

Charmed quarks ($c,\bar{c}$) are not produced frequently in the QGP, if their mass were large compared to the temperature. An experimental determination of the production rate of (multiple) $c\bar{c}$ pairs in nuclear collisions is extremely useful for assessing their contribution (via semileptonic decays) to the yield of non-resonant dileptons[81] in the mass range between about 0.5 and 3 GeV.

5.4 Deconfinement and Hadron Suppression

The key property of a thermalized QGP is deconfinement. Consequently, it is most important to verify this feature experimentally.

Suppression of charmonium production in heavy ion collisions was first suggested in ref. 96 to directly reflect deconfinement: In the early stage of a collision $\bar{c}c$-pairs are formed by the gluon-fusion process $gg \to c\bar{c}$. The distance between the two charmed quarks increases as they move through the QGP. Once they reach their binding radius inside the QGP, their mutual attraction is Debye-screened, hence they stay unbound. This occurs[97] near the transition temperature T_c for ψ' and χ_c, and at $T/T_c > 1.3$ for J/ψ. In pp collisions about 40% of the inclusive yield of J/ψ comes from χ_c decays,[98] this implies some J/ψ suppression already at T_c. Due to the large mass of charmed quarks the probability to create further thermal $c\bar{c}$-pairs in a QGP is small. Therefore, the formation of charmonia by recombination at the transition to confinement is very unlikely.

It is furthermore intuitively clear, that $c\bar{c}$-pairs with smaller (transverse) momenta stay longer inside the QGP, hence the suppression becomes more efficient.[97]

A search for such a suppression was undertaken by NA38.[99] Opposite charge dimuon spectra in the mass range $0.5 \leq M_{\mu\mu} \leq 5$ GeV were obtained from $6 \cdot 10^5$ pU, $8 \cdot 10^5$ O-Cu and $2.5 \cdot 10^6$ O-U collisions at 200 GeV/c/N. Preliminary data on S-U interactions at the same beam momentum are also available.[100] The opposite sign dimuons are free of background from meson decays for $M_{\mu\mu} \gtrsim 2.5$ GeV. This background was assumed to be equal to the flux of same charge dimuons, a standard,[82] but not necessarily well justified[81] assumption.

In fig. 35 background subtracted mass spectra are shown for two sets of O-U collisions which are characterized by the measured el.magn. transverse energy E_T. Events with $E_T < 33$ GeV are due to rather peripheral collisions, whereas those with $E_T > 82$ GeV are good candidates for the QGP. Both mass distributions are normalized to a fit of the non-resonant continuum to the parameterization $dN/dM_{\mu\mu} \propto e^{-M_{\mu\mu}/M_o}$, $M_o \sim 1.33$ GeV. The shape of the continuum is compatible with being independent of E_T and with the one found for pp collisions. This finding is non-trivial because of i) potential thermal components of the continuum in the case of a QGP (section 5.2), ii) other sources of dileptons, such as semileptonic decays of charmed particles, which are presumably suppressed in the QGP.

All contributions to the continuum may give rise to different shapes of the angular distributions of the muons such that acceptance corrections depend on assupmtions.

The number N_J of J/ψ resonances normalized to the continuum (N_c) in events with $E_T > 82$ GeV is significantly suppressed in fig. 35 relative to events with $E_T < 33$ GeV. More details on this correlation are given in fig. 36a, where the ratio N_J/N_c is displayed for O-Cu, O-U and S-U interactions.[100,101] The suppression becomes stronger for larger values of a scaling variable $E_T/B^{2/3}$, which is proportional to the energy density ε for a fixed target A. No dependence on E_T is measured for proton induced reactions.

To investigate the suppression as a function of transverse momentum p_T of the J/ψ a ratio $\bar{R} = S(E_{T1};p_T)/S(E_{T2};p_T)$ was defined, where $S(E_T;p_T) = [N_J(p_T)/N_c]_{E_T}$ reflects the suppression of J/ψ with transverse momentum p_T relative to the continuum ($1.6 < M_{\mu\mu} \leq 5.1$ GeV) in events with given transverse energy E_T. The measured ratio $\bar{R}$ is displayed in fig. 36b for O-U collisions with $E_{T1} > 68$ GeV and $E_{T2} < 38$ GeV.[101,102] A suppression factor R ~ 0.53 is obtained at $p_T = 0$, while the suppression vanishes at $p_T > 2.8$ GeV/c as predicted for a QGP.[102]

Presently, no dependence of $\bar{R}$ on p_T is found for J/ψ production in pU collisions.[100]

Before looking into attempts to explain these data without invoking a QGP, it is worth underlining that the early observation of such a predicted feature is a considerable experimental achievement. The extraction of a dimuon signal, virtually free of background, in an environment of extremely large numbers of mesons is by no means a trivial task.

There are essentially two types of non-QGP models which lead to an apparent suppression of charmonium in nuclear collisions. They are based on i) nuclear effects and ii) absorption in a dense hadron gas.

A dependence of the inclusive cross section for dilepton ($\ell\bar{\ell}$) production on the atomic mass A was established experimentally:[103] $r(\ell\bar{\ell}) = d\sigma(pA \rightarrow \ell\bar{\ell} + X)/d\sigma(pp \rightarrow \bar{\ell}\ell + X) \propto A^{\alpha(\ell\bar{\ell})}$, where α (cont.) = 1.0 for the continuum and $\alpha(J/\psi) = 0.95$. Consequently, one can estimate a relative suppression of J/ψ in pA collisions: $r(J/\psi)/r(\text{cont.}) \propto A^{-0.05}$. These features are not yet well understood, and it is not completely obvious how to iterate for collisions of nuclei including a dependence on E_T; nevertheless, it is felt that the observed suppression cannot fully be accounted for in this way.[101] There is also a measured dependence of α on p_T,[104] possibly due to multiple scattering of the incident partons off the target.[105] This was recently shown to cause a rather strong dependence on p_T of J/ψ suppression.[106]

Hadronic absorption models for charmonium suppression start from the survival probability P(x) at a distance x from the point of production. P(x) is proportional to $e^{-x/\lambda}$, where, $\lambda = (\sigma\rho)^{-1}$ is the mean free path of charmonium in a medium of hadrons h with a density ρ, and σ is the cross section for inelastic processes, such as $J/\psi + h \to X + Y,\ X,Y \neq J/\psi$. To derive quantitative predictions, one must estimate cross sections of generally unobservable processes, e.g. for the exothermic reaction $J/\psi + \rho \to D + \bar{D}$.[107] The densities ρ of all relevant hadrons must be determined in accordance with the measured transverse energy. Also the dependence of ρ on time due to hydrodynamic expansion should be taken into account. Last, but not least, one evaluates the time a $c\bar{c}$-pair needs to reach its binding radius, and the additional formation time which passes before it 'behaves like a hadron.' The formation time should agree with what is derived from modeling cascading processes.[55] A plausible adjustment of all ingredients leads to a reasonable reproduction of the observed J/ψ suppression;[107] usually rather high matter densities are needed.

A discrimination between all competing interpretations is likely to require measurements over a large solid angle of variations with the atomic masses of projectile and target, incident energy, and impact parameter.

An alternative method to search for color screening effects was proposed recently.[108] The idea is based upon detailed investigations[109] of proton production at $p_T \gtrsim 3$ GeV/c in pp collisions. So far, the data are only reproduced by QCD-inspired models assuming hard scattering of a 2-quark cluster ('diquark') from one proton off a parton from the other proton.[110] Since a diquark presumably owes its existence to the confinement of 3 valence quarks inside a nucleon, a QGP would cause a dissolution of diquarks, hence a reduction of inclusive cross sections for protons as well as neutrons and lambdas at $p_T \gtrsim 3$ GeV.

A compilation[108] of inclusive proton yields relative to positive pions is given in fig. 37 as function of p_T. Predictions obtained in the framework of lowest order QCD neglecting diquarks are included as well.[110] Very large suppression factors (>>2), especially at p_B ~70 GeV/c, are expected from these considerations. A further factor 2 is gained due to reduced yields of π^+ in nucleus-nucleus collisions, where about 50% of all nucleons are neutrons; on the other hand, only less than 50% of all diquarks may be affected by the QGP as a consequence of its formation time, spatial extension, and life time.[108]

As in the case of J/ψ suppression one has to evaluate quantitatively absorption processes in dense hadronic matter. In this respect it is encouraging that inclusive p/π^+ ratios are measured to be the same in pp and pA collisions.[111]

6. CONCLUSIONS

The subject of this review is a young field of research, whose virtual state was turned into reality by the availability of high energy ion beams late in 1986.

The goal is a better understanding of the phenomenon of confinement. It may be achieved by investigating a phase transition in nuclear collisions to a thermalized plasma of quarks and gluons. The experiments have to face the challenge of events with a few hundred secondary particles, a difficult task which has been accomplished in a remarkable fashion so far. These efforts are perfectly balanced by an increasing supply of theoretical ideas on QGP signatures and by refined calculations as well as by the flawless operation of the accelerators.

The first experiments making use of O and Si beams with momenta up to 15 GeV/c/N at BNL and of O and S beams at 60 and 200 GeV/c/N at CERN have already produced a wealth of data needed for a detailed understanding of basic event features. This is a vital step to tune simulation programs which are based upon the "conventional" physics of pp and pA collisions. One hopes then to prove the existence of a deconfined state of partons on the basis of incompatibilities of data with these simulations.

Measurements of cross sections established a rather large contribution from electro-magnetic dissociation which limits the lifetime of colliding nuclear beams at high energies; it may also be a valuable source of pairs of heavy leptons.

Spectra of energy flow close to the beam direction and of transverse energy, as well as of multiplicity and rapidity distributions reflect the dominance of collision geometry. They are well reproduced by current simulation programs which are based on superpositions of pp collisions.

Appropriate triggers for central collisions were designed on the basis of collisions geometry. In these violent interactions, projectile and target overlap completely such that most of their kinetic energy is transformed into secondary particles, a feature called "stopping." Rather model dependent estimates suggest that energy densities more than 10 times the ones of nuclei are reached in central collisions. This meets theoretical predictions for a phase transition. Extrapolations indicate, that with Pb beams at 200 GeV/c/N and especially at higher energies, conditions become even more favorable. One should also keep in mind that high energy densities may be generated in some $\overset{(-)}{p}p$ collisions.

Pion interferometry may have provided first hints for an expanding source in central collisions.

A steepening of $d\sigma/dp_T^2$ at $p_T < 0.25$ GeV/c was observed in central collisions of oxygen and protons with heavy targets. Assuming thermalization, this may correspond to a component of lower temperatures as expected from an expanding system. On the other hand, the average transverse momentum is independent of presently accessible particle multiplicities. It is probably a measure both of the temperature and collective flow at freeze-out, which answers the question raised at the end of section 2.1.

There are no firm data yet on yields of direct real or virtual photons which are believed to signal the presence of a QGP and to "measure" its temperature.

The generic feature of a QGP is the deconfinement of partons. Its most direct verification was to be based on measurements of J/ψ suppression. Similarly, a 'melting' of diquarks should result in reduced relative production rates of protons and lambdas at high transverse momentum.

The outstanding experimental result is therefore the observed strong suppression of J/ψ resonances in central O-U and S-U collisions relative to the dilepton continuum, and its dependence on transverse momentum. Formation of a QGP provides an economic, rather quantitative interpretation of the data. Good agreement is also found with more conventional models assuming absorption in very dense hadronic matter, eventually combined with nuclear effects.

One is lead to conclude that only detailed studies of many aspects of suppression mechanisms, i.e. of a dependence on kinematic variables, on the centrality of the collision as well as on the masses of colliding nuclei (including protons) and on the beam energy, will unravel competing mechanisms.

The case of J/ψ suppression may very well turn out to be typical for many proposed QGP signatures. The tedious task of systematic measurements and the non-uniqueness of interpretations of subsets of data are a consequence of the fact that one is searching for a new transient phenomenon rather than for e.g. a particle with predicted quantum numbers. In this framework one ought to remember that a decade of experimentation and analysis was needed to understand the phenomenon of deep inelastic scattering of hadrons on a satisfactory level.

Again, H_2O molecules may provide a useful analogy: Three different snowflakes are shown in fig. 38.[112)] Deciphering the secrets of the QGP is equivalent to determining the properties of water or steam from measurements on snowflakes. It is evident that the symmetry of any given snowflake originates from the underlying symmetry of water molecules. However, no two snowflakes are alike. Differences are caused by individual space-time histories, i.e., by different paths through a turbulent atmosphere, amplified by non-linear "clustering" processes. Most probably, fluctuations in space-time evolution generate also large variations of certain features of nuclear collisions from which the underlying pattern of the QGP must be disentangled.

While rapid progress in this new field of strong interactions physics continues[113] and the confidence to reach a phase transition finds its support in present data, one may still feel for some time as Newton probably did as he, in a letter, imagined himself "... playing on the sea shore ... now and then finding a smoother pebble or prettier shell than ordinary, while the great ocean of truth lay all undiscovered before me."

Acknowledgments:

I gratefully acknowledge discussions with many colleagues, a critical reading of the manuscript by S. Gavin and the diligent work of A. Fitzgerald.

REFERENCES

1. Lucretius, De rerum natura, Penguin Books.
2. J.H. Applegate et al., Phys. Rev. D35 (1987) 1151.
3. L.D. McLerran, Rev. Mod. Phys. 58 (1986) 1021.
4. K. Kajantie and L.D. McLerran, Ann. Rev. Nucl. Part. Sci. (1987), p.293.
5. K. Guettler et al., Phys. Lett. 64B (1976) 111.
6. R. Hagedorn, Rivista Nuov. Cim. 6 (1983) 10.
7. Y.A. Tarasov, Sov. J. Nucl. Phys. 42 (1985) 260.
   W.M. Geist, LBL-25425.
8. R. Hagedorn, Nuov. Cim. 56 (1968) 1027.
9. a) see e.g. F. Karsch, Z. Phys. C 38 (1988) 147.
   b) P. Bacilieri et al., Phys. Rev. Lett. 61 (1988) 1545.
10. See e.g. M. Gyulassy, Progr. Part. & Nucl. Phys. 15 (1985) 403.
11. B. Berg et al., Z. Phys. C 31 (1986) 167.
12. P.V. Ruuskanen, Act. Phys. Pol. B18 (1987) 551.
13. K. Redlich and H. Satz, Phys. Rev. D33 (1986) 3747.
14. See e.g. H. Ehtamo et al., Z. Phys. C 18 (1983) 341, and A. Bialas and W. Czyz, Phys. Rev. D31 (1985) 198.
15. L. van Hove and A. Giovannini, CERN-TH. 4957/88.
16. J.D. Bjorken, Phys. Rev. D27 (1983) 140.
17. I. Otterlund et al., Z. Phys. C 20 (1983) 281.
18. H. von Gersdorff et al., Phys. Rev. D34 (1986) 794.
    J.P. Blaizot, Act. Phys. Pol. B18 (1987) 659.
19. P. Barnes et al., Phys. Lett. 206B (1988) 146.
20. A. Bamberger et al., Phys. Lett. 205B (1988) 58.
21. See e.g. E.O. Abdrahmanov et al., Z. Phys. C5 (1980) 1.
22. P. Yepes and R. Zybert, Proceedings 23rd Rencontre de Moriond, Les Arcs, France, 13-19 March 1988.
23. D. Olson et al., Phys. Rev. C24 (1981) 1529.
24. J.C. Hill et al., Phys. Rev. Lett. 60 (1988) 999.

25. a) G. Baur and C.A. Bertulani, Phys. Rev. C 34 (1986) 1654.
C.A. Bertulani and G. Baur, Nucl. Phys. A458 (1986) 725.
b) G. Baur and C.A. Bertulani, Phys. Rev. C37 (1987) 836.

26. B. Berthier et al., Phys. Lett. 193B (1987) 417.

27. J. Hüfner, Phys. Rep. C125 (1985) 129.

28. I. Otterlund, Z. Phys. C38 (1988) 65.

29. A.S. Goldhaber, Phys. Lett. 53B (1974) 306.

30. R. Albrecht et al., Phys. Lett. 199B (1987) 297.

31. B. Nilsson-Almqvist and E. Stenlund, Comp. Phys. Comm. 43 (1987) 387.

32. R.J. Glauber, Lectures in Theoretical Physics, Vol. 1, p. 315.
W.E. Brittain, L. G. Dunham, (eds.), New York, Interscience 1959.

33. P. Yepes, Ph.D. thesis, Univ. of Santiago, Spain, 1988.
I. Sakrejda, Proceedings of the XIXth International Symposium on Multiparticle Dynamics, Arles, France, June 1988.

34. Y. Takahashi, Nucl. Phys. A478 (1988) 675c.

35. O. Badawy, priv. comm.

36. A. Capella et al., Phys. Rev. D35 (1987) 2921.
A. Capella et al., Z. Phys. C33 (1987) 541.

37. J. Rafelski et al., UCT-TP81/1987.

38. H. Ströbele, Z. Phys. C38 (1988) 89.

39. M.I. Adamovich et al., Phys. Lett. 201B (1988) 397.

40. a) J.L. Bailly et al., Z. Phys. C35 (1987) 301.
b) C. De Marco et al., Phys. Rev. D26 (1987) 1019.

41. H.R. Schmidt, Z. Phys. C38 (1988) 109.

42. I. Lund, Z. Phys. C38 (1988) 51.

43. a) J. Whitmore, Phys. Rep. 27C (1976) 215.
b) W. Thomé et al., Nucl. Phys. B129 (1977) 370.

44. L. van Hove, Z. Phys. C27 (1985) 135.

45. M. Adamus et al., Phys. Lett. 185B (1987) 200, and refs. therein.

46. T. Abott et al., Phys. Lett. 197B (1987) 285.

47. C.P. Remsberg and M.J. Tannenbaum, Z. Phys. C38 (1988) 35.

48. W. Heck, Z. Phys. C38 (1988) 19.

49. C.W. Fabjan, CERN-EP/88-73.

50. A. Bamberger et al., Phys. Lett. 184B (1987) 271.

51. P. Braun-Munzinger, Z. Phys. C38 (1988) 45.

52. T. Akesson et al., Z. Phys. C38 (1988) 383.

53. F. Lamarche, Proceedings 23rd Rencontre de Moriond, 13-19 March 1988, Les Arcs, France.

54. J. Schukraft, Proceedings of the XIXth. International Symposium on Multiparticle Dynamics, Arles, France, June 1988, and CERN-EP/88-141.

55. J. Ranft, Phys. Rev. D37 (1988) 1842.

56. T. Akesson et al., Z. Phys. C38 (1988) 397.

57. See e.g. P.V. Ruuskanen, JYFL 9/88.

58. R. Hanbury-Brown and R. Twiss, Phil. Mag. 45 (1954) 663.

59. See e.g. G. Goldhaber, Proc. LESIP I, ed. D.K. Scott and R.M. Weiner (Bad Honnef, 1984).

60. A. Bamberger et al., Phys. Lett. 203B (1988) 320.

61. K. Kolehmainen and M. Gyulassy, Phys. Lett. 180B (1986) 203.

62. M. Gyulassy and S.S. Padula, LBL-26077.

63. S. Pratt, Phys. Rev. D33 (1986) 1314.
G.F. Bertsch, Detecting the Quark-Gluon Plasma, Michigan State Preprint, June 1988.
Y. Hama and S.S. Padula, Phys. Rev. D37 (1988) 3237.

64. M. Kataja et al., Phys. Rev. D34 (1986) 2755.

65. H.W. Bartels, Z. Phys. C38 (1988) 85.

66. T.W. Atwater et al., Phys. Lett. 199B (1987) 30.

67. K. Guettler et al., Nucl. Phys. B116 (1976) 77.

68. A. Albrecht et al., Phys. Lett. 201B (1988) 390.

69. E.V. Shuryak, Phys. Lett. 207B (1988) 345.

70. W. Bell et al., Z. Phys. C27 (1985) 191.

71. H.G. Fischer, Z. Phys. C38 (1988) 105.

72. J.W. Cronin et al., Phys. Rev. D11 (1975) 3105.

73. M. Lev and B. Petersson, Z. Phys. C21 (1983) 155.

74. H.W. Bartels, Proceedings 23rd Rencontre de Moriond, 13-19 March 1988, Les Arcs, France.

75. T. Alexopoulos et al., Phys. Rev. Lett. 60 (1988) 1622.

76. A. Breakstone et al., Phys. Lett. 183B (1987) 227.
A. Breakstone et al., Z. Phys. C33 (1987) 333.
A. Breakstone et al., Europhys. Lett. 7 (1988) 131.

77. G. Arnison et al., Phys. Lett. 118B (1982) 167.

78. L.D. McLerran and V.T. Toimela, Phys. Rev. D31 (1985) 545.
R.C. Hwa and K.Kajantie, Phys. Rev. D32 (1985) 1109.
K. Kajantie et al., Phys. Rev. D34 (1986) 2746.

79. See e.g. M.I. Gorenstein, Phys. Lett. 192B (1978) 19.

80. T. Akesson et al., Phys. Lett. 192B (1987) 463.
W. Willis, Nucl. Phys. A478 (1988) 151c.

81. H.G. Fischer and W.M. Geist, Z. Phys. C19 (1983) 159.

82. I.R. Kenyon, Rep. Progr. Phys. 45 (1982) 1261.

83. G. Roche et al., Phys. Rev. Lett. 61 (1988) 1069.

84. R. Santo, Proceedings of "Quark Matter '88", Lenox, Mass. USA, Sept. 1988.

85. P. Koch et al., Phys. Rep. C142 (1986) 167.

86. T. Sjöstrand, Int. J. Mod. Phys. A3 (1988) 751 and refs. therein.

87. See e.g. H.W. Barz et al., Nucl. Phys. A484 (1988) 661 and
G. Baym, Nucl. Phys. A479 (1988) 27c, and refs. therein.

88. Y. Miake and G.S.F. Stephans, Z. Phys. C38 (1988) 135.

89. C.M. Ko and L. Xia, Phys. Rev. C38 (1988) 179.

90. K. Miyano et al., KEK preprint 87-160 (Feb. 1988).

91. J. Rafelski, Phys. Lett. 207B (1988) 371.

92. G. Vesztergombi, Z. Phys. C38 (1988) 125.

93. S. Abatzis et al., Proceedings 23rd Rencontre de Moriond,
Les Arcs, France, 1988.

94. NA36, priv. comm.

95. Ch. Alcock and A. Olinto, Fermilab-Pub-88/58-A, and refs. therein.

96. T. Matsui and H. Satz, Phys. Lett. 178B (1986) 416.

97. See e.g. F. Karsch et al., Z. Phys. C37 (1988) 617.

98. Y. Lemoigne et al., Phys. Lett. 113B (1982) 509.

99. M.C. Abreu et al., Z. Phys. C38 (1988) 117 and CERN-EP/88-25.

100. See e.g. L. Kluberg, Discussion Meeting on Lead Beam
Experiments at the SPS, CERN, April 28-29, 1988.

101. See e.g. F. Karsch and R. Petronzio, Phys. Lett. 193B (1988) 105 and Z. Phys. C37 (1988) 627.

102. H. Satz, BI-TP88/10.

103. a) J. Badier et al., Z. Phys. C20 (1983) 101.
b) P. Bordalo et al., Phys. Lett. 193B (1987) 368.

104. S. Katsanevas et al., Phys. Rev. Lett. 60 (1988) 2121.
P. Bordalo et.al., Phys. Lett. 193B (1987) 373.

105. C. Michael and G. Wilk, Z. Phys. C10 (1981) 169.
G.T. Bodwin et al., Phys. Rev. Lett. 47 (1981) 1799.

106. S. Gavin and M. Gyulassy, LBL-25663.

107. S. Gavin et al., Phys. Lett. 207B(1988) 257.
J. Ftacnik et al., CERN-TH.5090/88, and refs. therein.

108. W.M. Geist, Phys. Lett. 211B (1988) 233.

109. A. Breakstone et al., Phys. Lett. 147B (1984) 237.
A. Breakstone et al., Z. Phys. C35 (1987) 157.
A. Breakstone et al., Z. Phys. C36 (1987) 567.

110. S. Ekelin and S. Fredriksson, Phys. Lett. 149B (1984) 509.
A. Breakstone et al., Z. Phys. C28 (1985) 335.
V.T. Kim, Mod. Phys. Lett. A9 (1988) 909.

111. D. Antreasyan et al., Phys. Rev. D19 (1979) 764.

112. J. Gleick, Chaos: Making of a New Science, (Viking, 1987).

113. Proceedings of "Quark Matter 88", Lenox, Mass., Sept. 1988 and "Hadronic Matter in Collision", Tuscon, Arizona, October 1988.

Figure Captions

1. Invariant cross section for π^+ versus p_T at different cms energies; the solid curve is a fit to exp $(-bm_T)$ for $p_T < 0.4$ GeV/c.
2. Phase diagram of strongly interacting matter.
3. Schematic representation of the space-time history of AA collisions.
4. Schematic representation of a central B-A collisions.
5. Experimental set-up of WA80.
6. Experimental set-up of NA38.
7. Experimental set-up of NA34.
8. Experimental set-up of E802.
9. The modified Ω' spectrometer of WA85.
10. Experimental set-up of NA35.
11. Experimental set-up of NA36.
12. The square root of a) the charge changing cross section (σ_m) and b) the inelastic cross section (σ_{prod}) for nuclear collisions as function of $A^{1/3} + B^{1/3}$ ($=A_T{}^{1/3} + A_p{}^{1/3}$) from ref. 22.
13. The measured cross section $\sigma(O\ {}^{197}Au \rightarrow {}^{196}Au + X)$ as function of the beam energy per nucleon and a theoretical prediction.
14. Distribution of projected polar angles of He-fragments.
15. Energy spectra measured in the Zero-Degree Calorimeter (ZDC) in oxygen induced reactions. Histograms give the results of the Fritjof model.
16. Energy spectra measured at $\theta < 0.4°$, in arbitrary units.
17. a) Scaled multiplicity distribution of shower particles and a prediction (solid line) from the Dual-Parton model. Also included is the KNO shape for pp collisions (dashed line).
    Scaled multiplicity distributions for negative particles from O-Au collisions (b) and O-Cu collisions (c).
18. The average number of shower particles as function of the number of participating projectile protons.
19. Corrected rapidity distributions for negative particles from central O-Au collisions.
20. Pseudorapidity distributions for high multiplicity events from EMU7 (a) and EMU1 (b).
21. Average number of baryons per event as function of pseudorapidity from oxygen induced reactions at 60 GeV/c/N (a), 200 GeV/c/N (b) and from proton induced interactions (c).

22. The transverse energy spectra measured in O-Au collisions at three different beam momenta.

23. Transverse energy spectra as function of $x = E_T/E_{Tmax}$ at 200 GeV/c/N (a) and 60 GeV/c/N .

24. Transverse energy distributions from oxygen induced reactions at 200 GeV/c/N . The shaded bands represent DPM (IRIS) predictions.

25. Transverse energy spectra in the range $-0.1 < 4 \leq 2.9$ from sulfur induced collisions at 200 GeV/c/N.

26. Normalized differential cross sections dE_T/dy from pPb collisions at 200 GeV/c/N for various values of E_T. The dashed lines represent inclusive pp collisions.

27. See fig. 26, but for oxygen induced reactions at 60 GeV/c/N (a) and 200 GeV/c/N (b).

28. Correlation function $C(q_1, q_2)$ as function of Q_T (for $Q_L < 100$ MeV) for 3 different rapidity intervals (a,b,c) and from the Fritjof model (d).

29. Comparison of Gaussian (a) and Kolehmainen-Gyulassy (b) source parameters for different rapidity intervals.

30. a) Transverse momentum distribution for central O-Au collisions and a fit to a two temperature thermal model (solid line).
    b) Invariant cross sections for π^o as function of p_T for proton and oxygen induced reactions. Solid lines and histograms correspond to exponential fits and predictions from Fritjof, respectively.

31. Theoretical prediction for the dependence of $< p_T >$ on the normalized rapidity density for AA Collisions.

32. Inverse slope of the differential cross section $d\sigma/dp_T^2$ as function of p_T for negative particles as function of E_T.

33. Invariant mass distribution for $\overline{\Lambda}$ and Λ obtained from S-W collisions at 200 GeV/c/N.

34. A reconstructed event obtained from a central collision of sulfur with a heavy target; it contains the decay of a neutral particle shown separately.

35. Dimuon mass spectra from O-U collisions for two ranges of E_T, normalized to the continuum.

36. a) Number of J/Ψ resonances relative to the continuum as function of E_T/(atomic mass of target)$^{2/3}$ at 200 GeV/c/N.
    b) The ratio $\overline{R}$ (see text) as function of the transverse momentum of J/Ψ for O-U collisions at 200 GeV/c/N, and a prediction assuming QGP formation.

37. A compilation of inclusive $p/\pi^+(\bar{p}/\pi^-)$ ratios as function of p_T from fixed target (a) and ISR (b) experiments. A QCD prediction neglecting diquarks is included (solid line).

38. Three snowflakes.

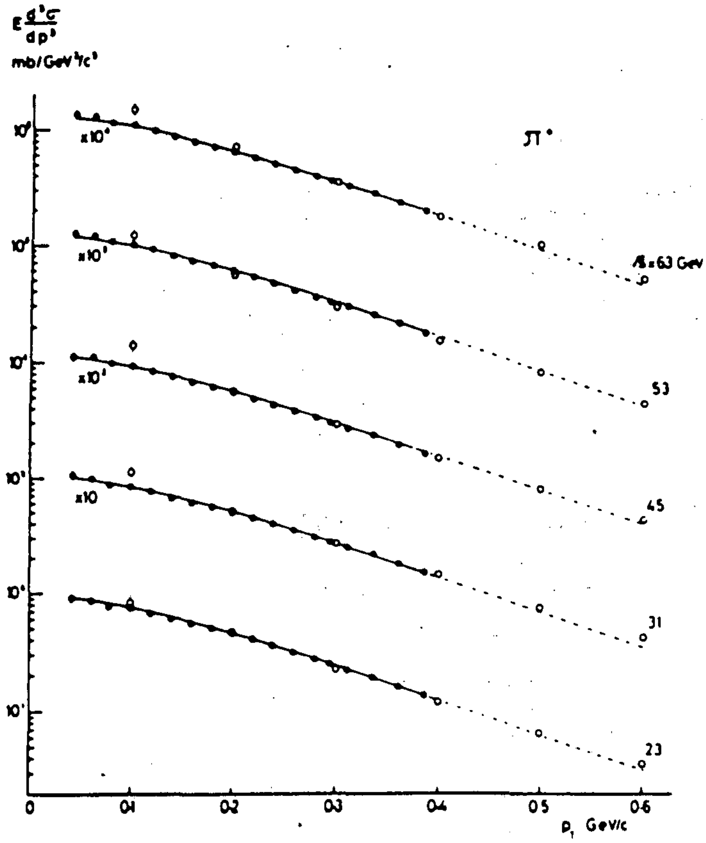

Fig. 1

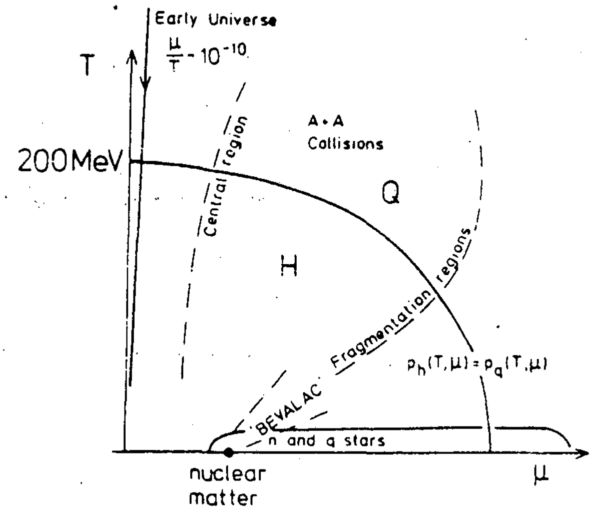

Fig. 2

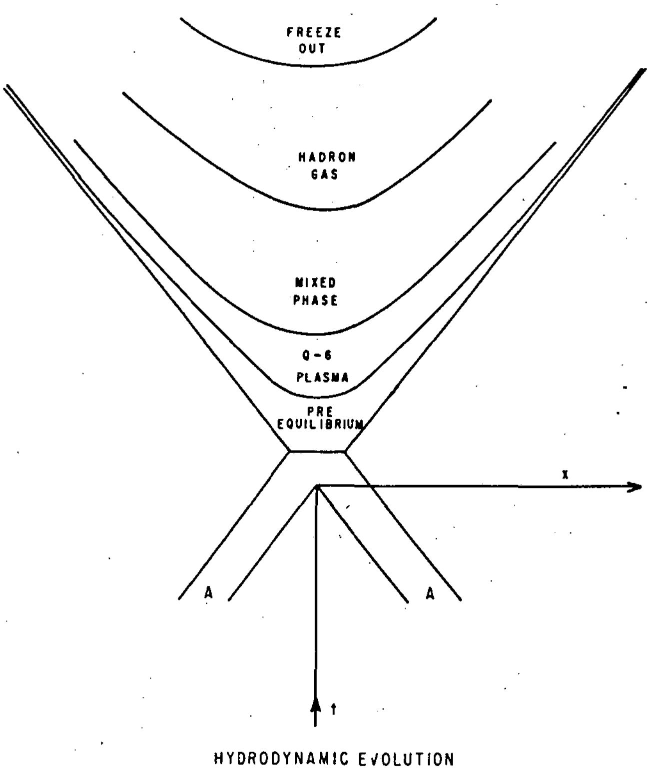

Fig. 3

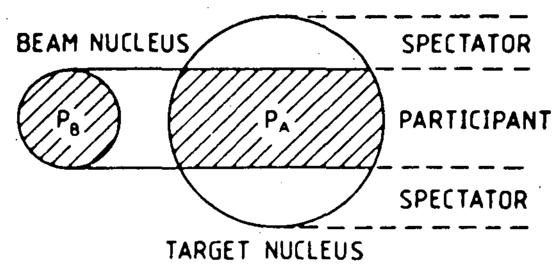

Fig. 4

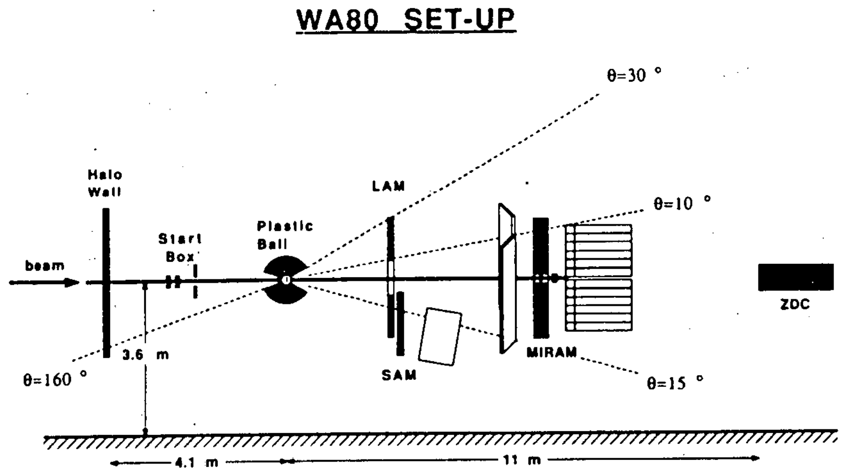
WA80 SET-UP
θ=30 °
Halo
Wall
LAM
θ=10 °
Plastic
Ball
Start
Box
beam
ZDC
θ=160 °
3.6 m
SAM
MIRAM
θ=15 °
4.1 m
11 m

Fig. 5

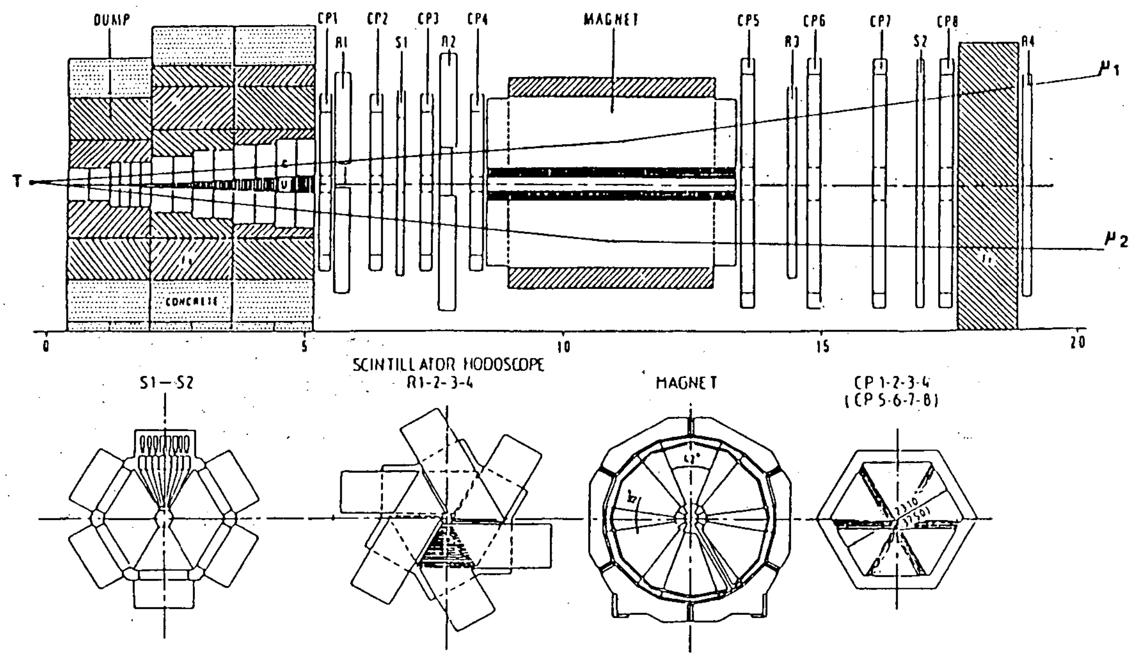
DUMP
CP1
CP2
CP3
CP4
MAGNET
CP5
CP6
CP7
CP8
R1
S1
R2
R3
S2
R4
T
CONCRETE
0
5
10
15
20
SCINTILLATOR HODOSCOPE
S1—S2
R1-2-3-4
MAGNET
CP 1-2-3-4
(CP 5-6-7-8)

Fig. 6

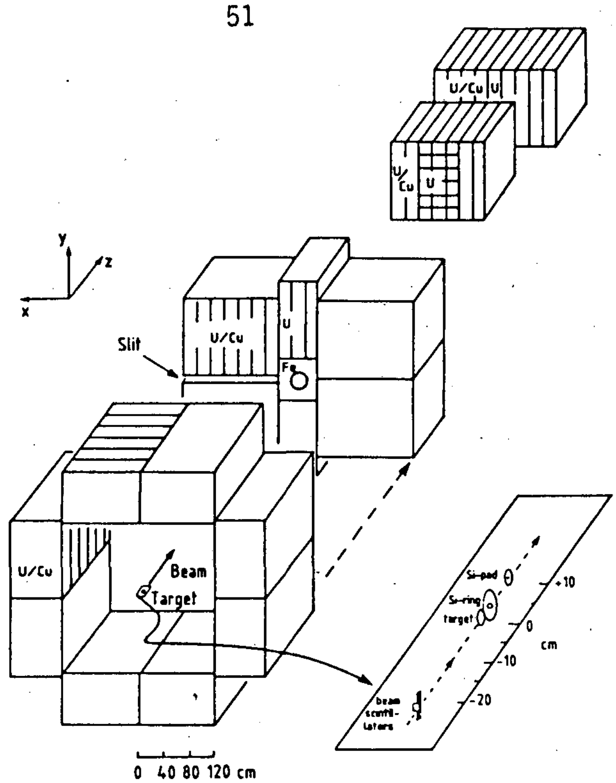
U/Cu
U
y
z
x
Slit
Fe
Beam
Target
Si-pad
Si-ring
target
+10
0
cm
-10
-20
beam scintil-lators
0 40 80 120 cm

Fig. 7

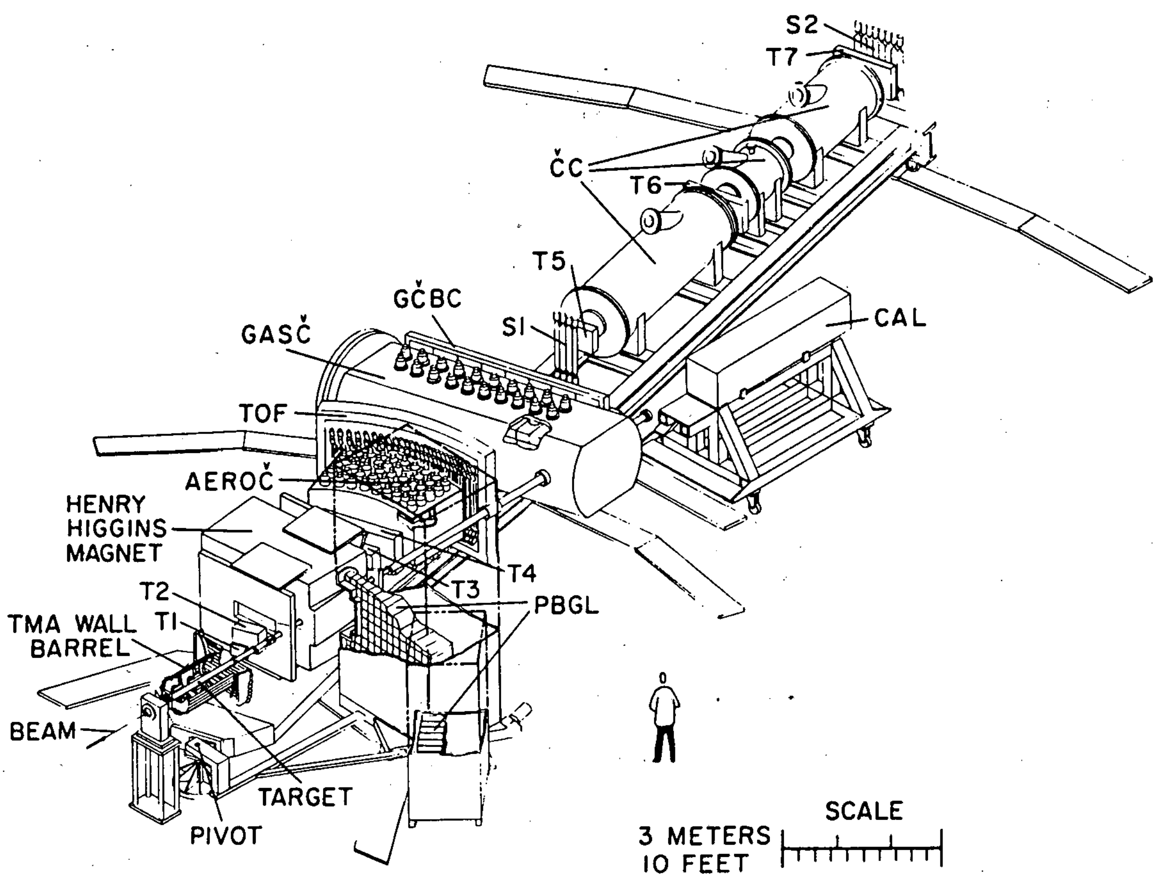
S2
T7
ČC
T6
T5
GČBC
GASČ
SI
CAL
TOF
AEROČ
HENRY HIGGINS MAGNET
T4
T3
T2
PBGL
TMA WALL
TI
BARREL
BEAM
TARGET
PIVOT
SCALE
3 METERS
10 FEET

Fig. 8

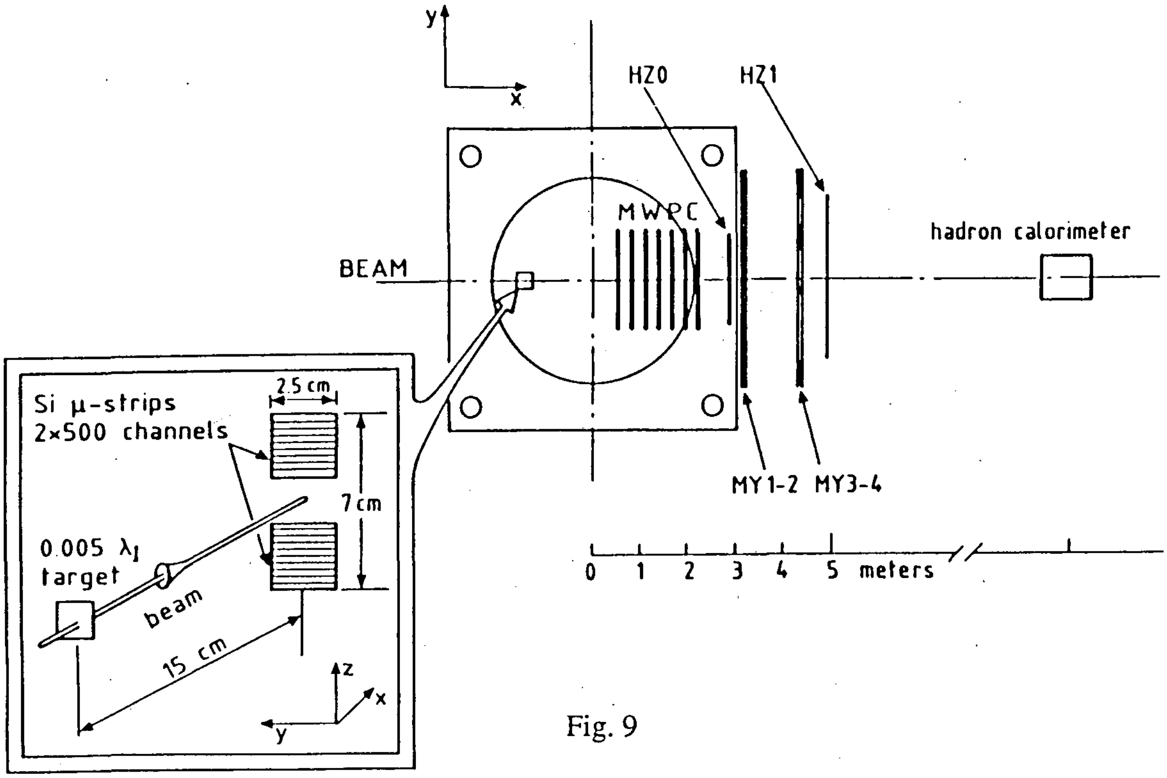

Fig. 9

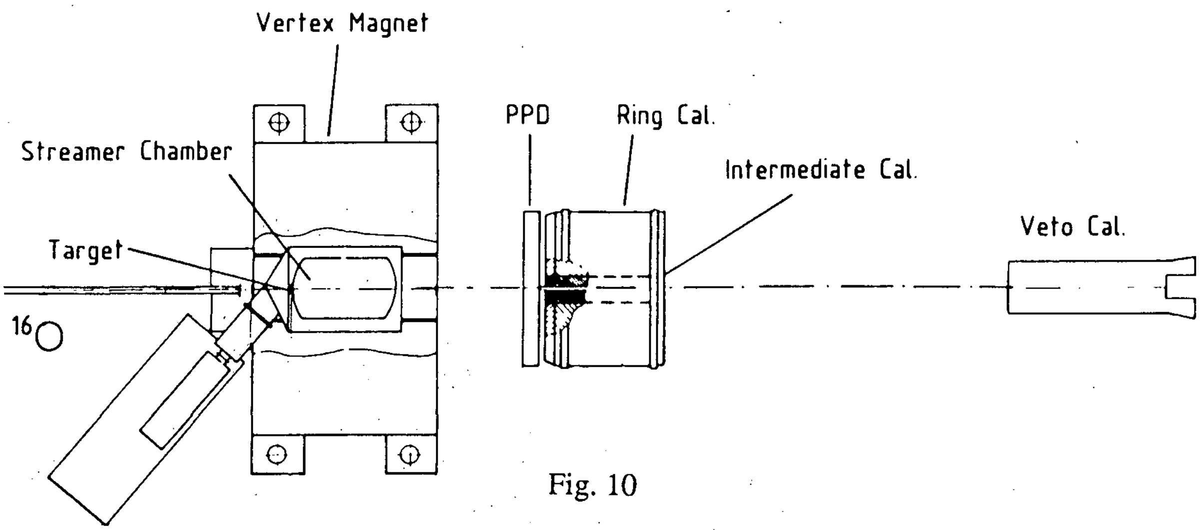

Fig. 10

BG Beam Geometry Counters
BT, BV Si Beam Tag, Beam Veto
Tg Targets
U_1, U_2, U_3, W_2 MWPC's
D_1-D_6 Drift Chambers
H_1, H_2 Hodoscopes
M_1, M_2 Magnets
IGD Intermediate Gamma Detector
INC Intermediate Neutral Calorimeter
Fč Forward Čerenkov
FGD Forward Gamma Detector
FNC Forward Neutral Calorimeter

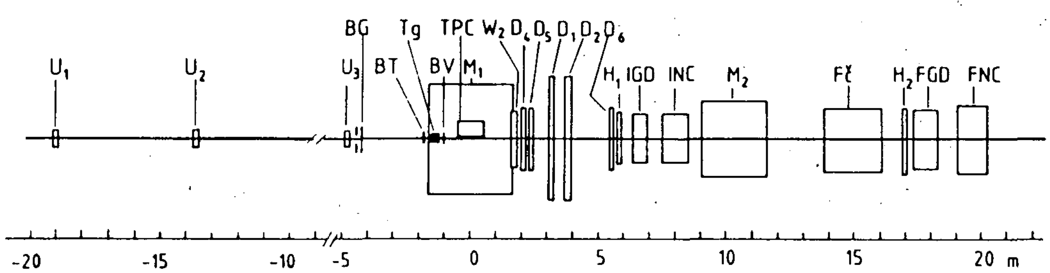

Fig. 11

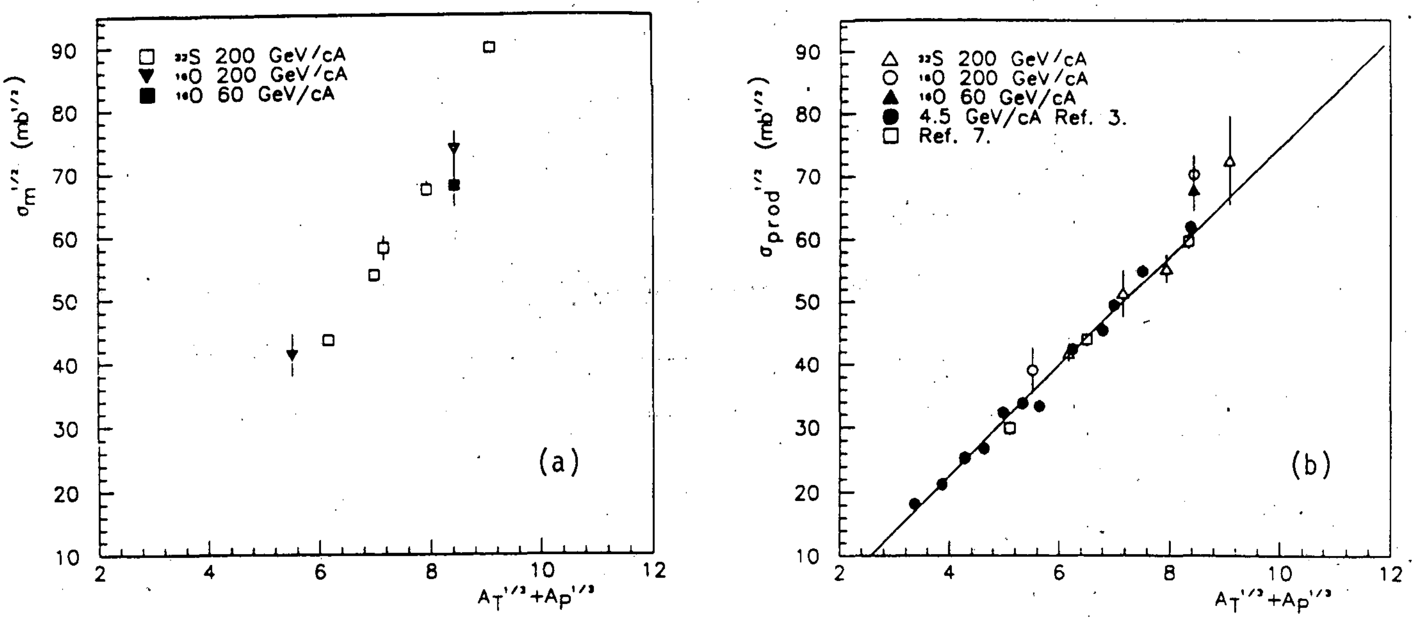

□ 32S 200 GeV/cA
▼ 16O 200 GeV/cA
■ 16O 60 GeV/cA
$\sigma_m^{1/2}$ (mb$^{1/2}$)
(a)
$A_T^{1/3}+A_P^{1/3}$
△ 32S 200 GeV/cA
○ 16O 200 GeV/cA
▲ 16O 60 GeV/cA
● 4.5 GeV/cA Ref. 3.
□ Ref. 7.
$\sigma_{prod}^{1/2}$ (mb$^{1/2}$)
(b)
$A_T^{1/3}+A_P^{1/3}$

Fig. 12

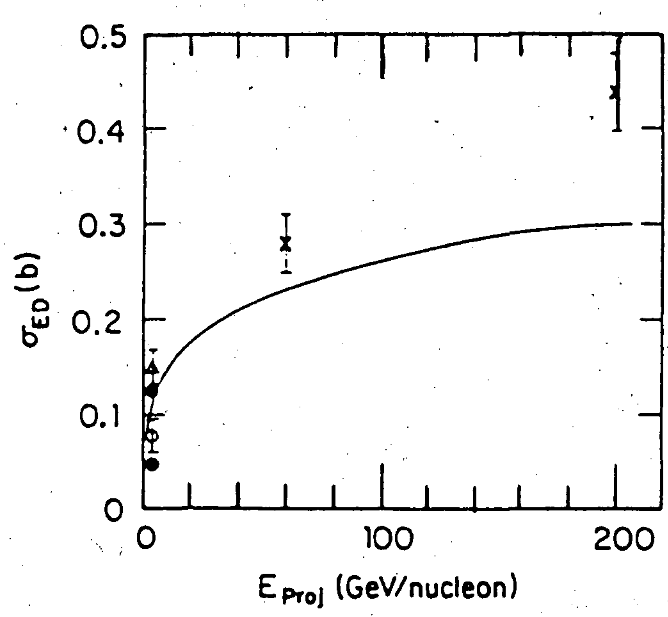

σ_{ED}(b)
E_{Proj} (GeV/nucleon)

Fig. 13

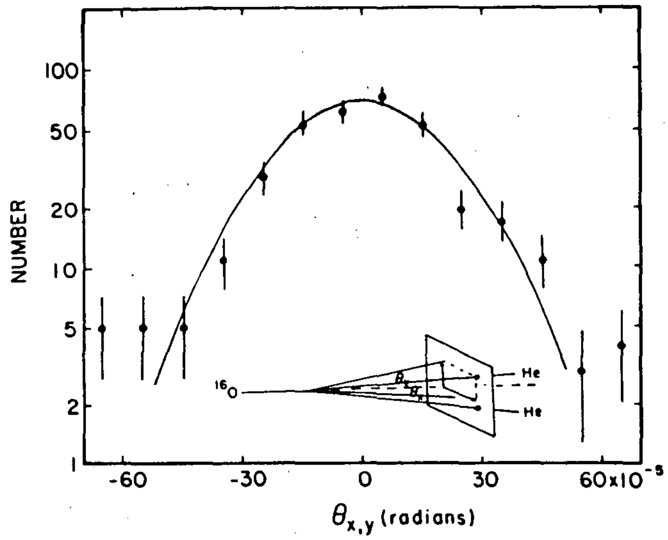

Fig. 14

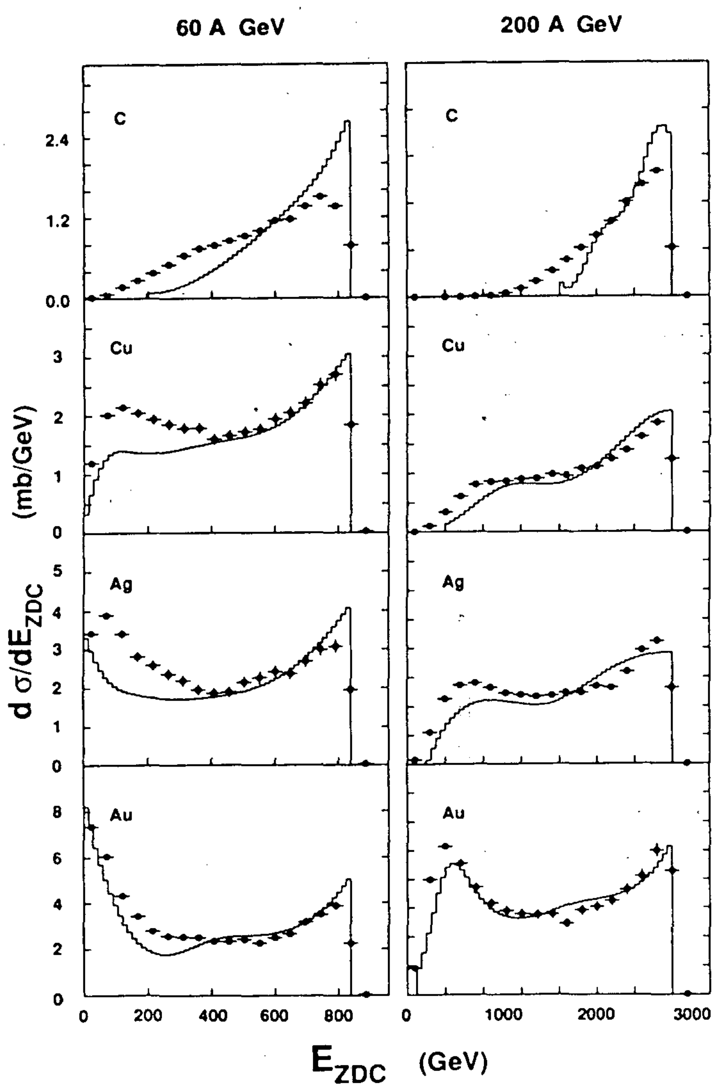

Fig. 15

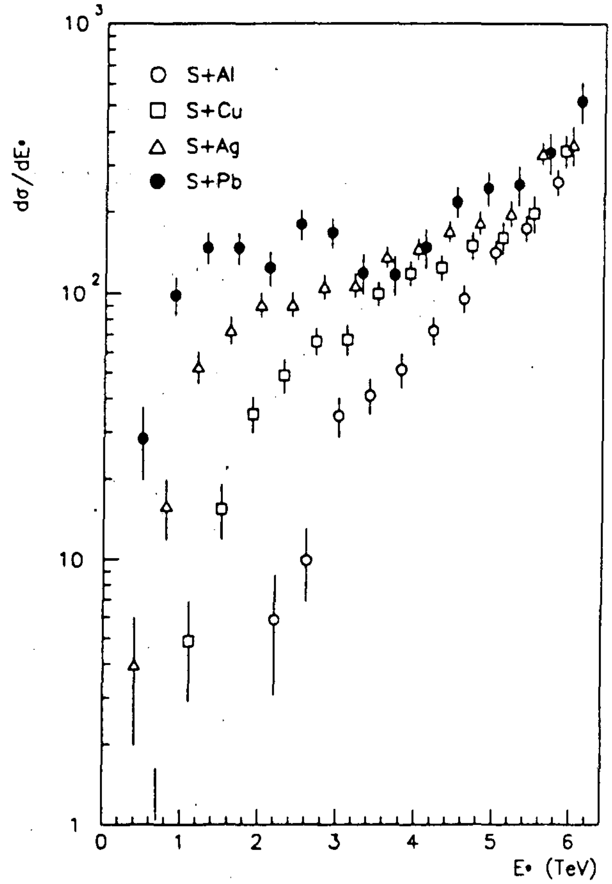

Fig. 16

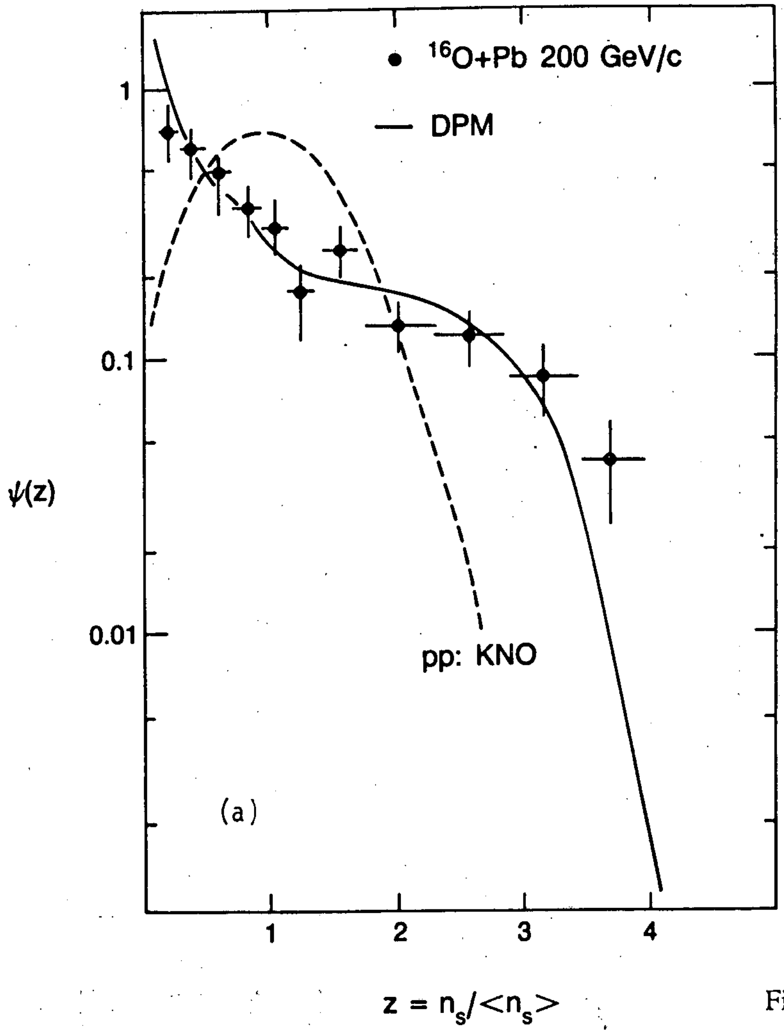

^{16}O+Pb 200 GeV/c
DPM
pp: KNO
(a)
ψ(z)
1
0.1
0.01
1
2
3
4
z = $n_s/\langle n_s \rangle$

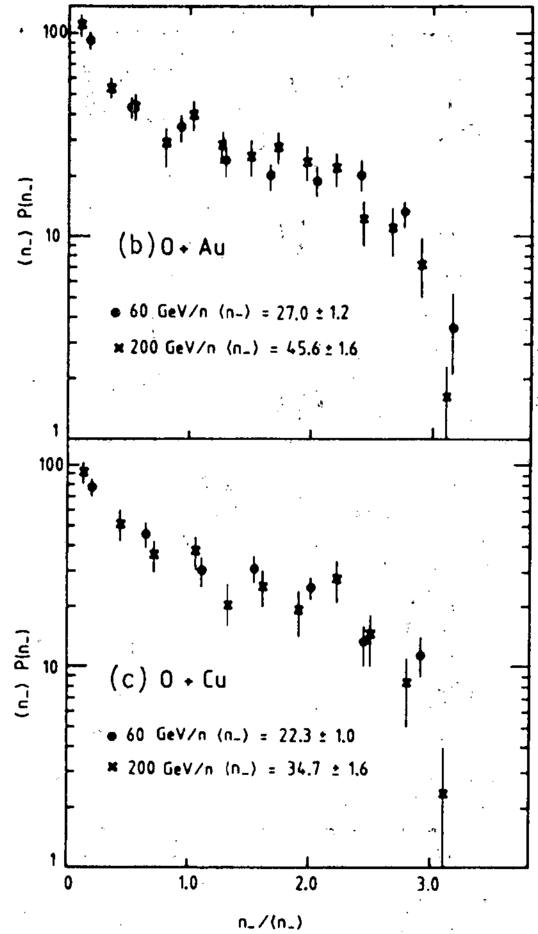

(b) O + Au
60 GeV/n ⟨n₋⟩ = 27.0 ± 1.2
200 GeV/n ⟨n₋⟩ = 45.6 ± 1.6
(c) O + Cu
60 GeV/n ⟨n₋⟩ = 22.3 ± 1.0
200 GeV/n ⟨n₋⟩ = 34.7 ± 1.6
⟨n₋⟩ P(n₋)
n₋/⟨n₋⟩

Fig. 17

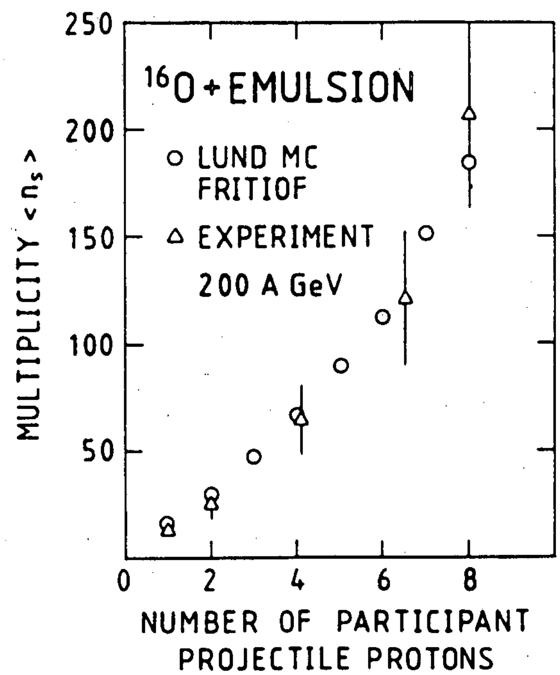

^{16}O + EMULSION
LUND MC FRITIOF
EXPERIMENT
200 A GeV
MULTIPLICITY ⟨n_s⟩
NUMBER OF PARTICIPANT PROJECTILE PROTONS

Fig. 18

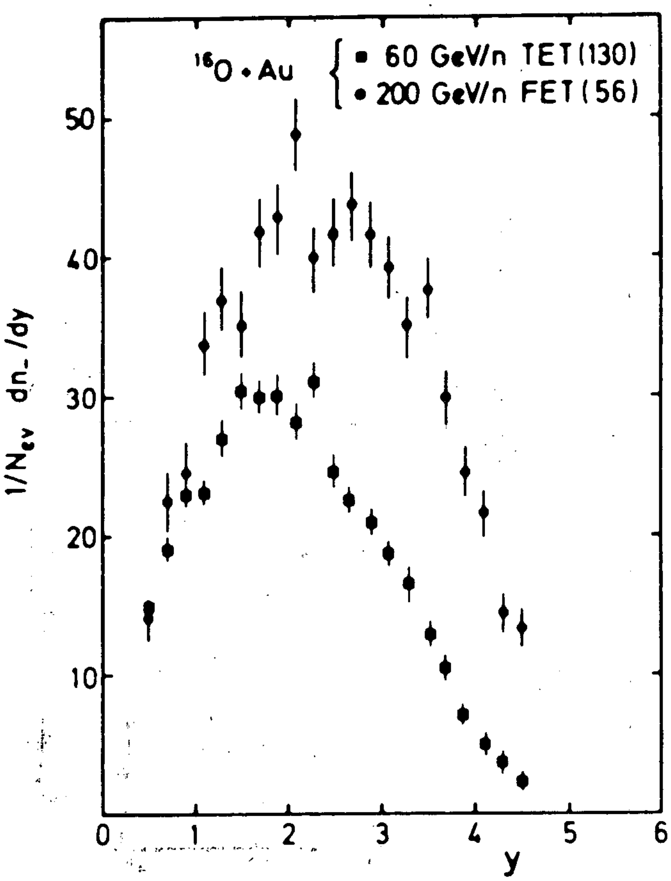

^{16}O + Au
■ 60 GeV/n TET(130)
● 200 GeV/n FET(56)
1/N$_{ev}$ dn$_-$/dy
y

Fig. 19

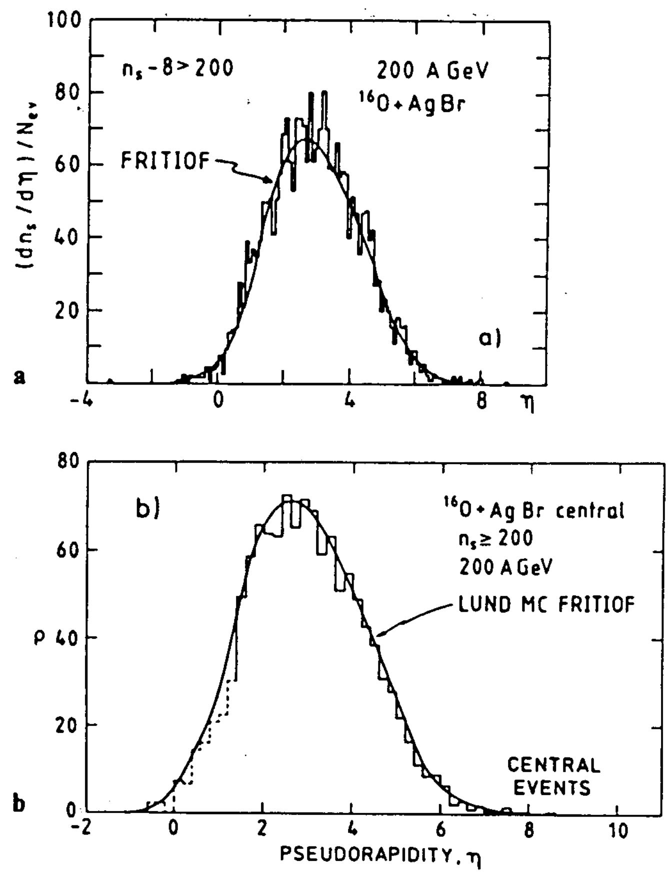

n$_s$ - 8 > 200
200 A GeV
^{16}O + AgBr
FRITIOF
(dn$_s$ / dη) / N$_{ev}$
a)
a
η
b)
^{16}O + Ag Br central
n$_s$ ≥ 200
200 A GeV
LUND MC FRITIOF
ρ
CENTRAL EVENTS
b
PSEUDORAPIDITY, η

Fig. 20

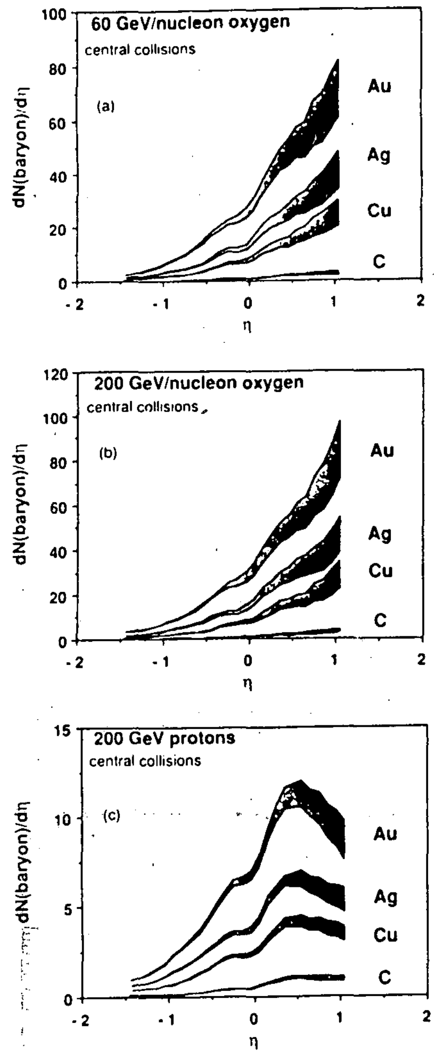

Fig. 21

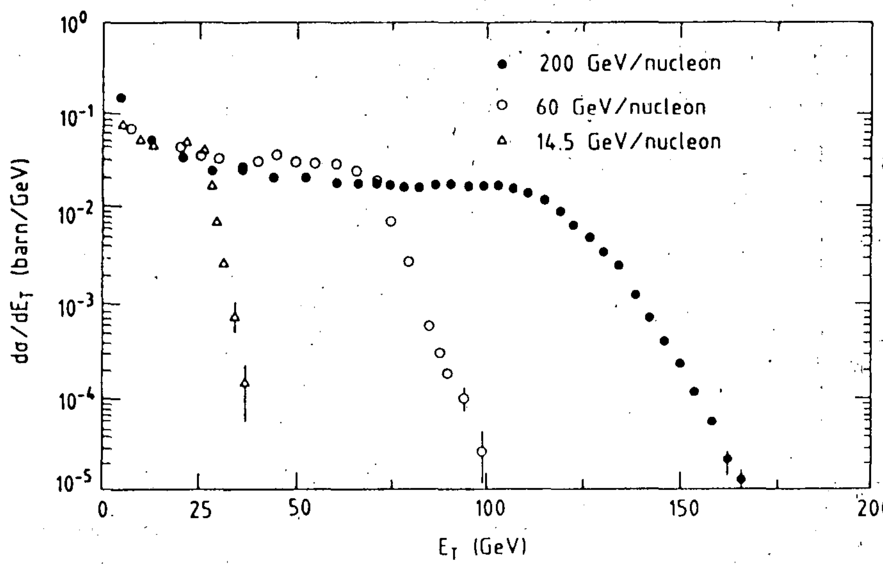

Fig. 22

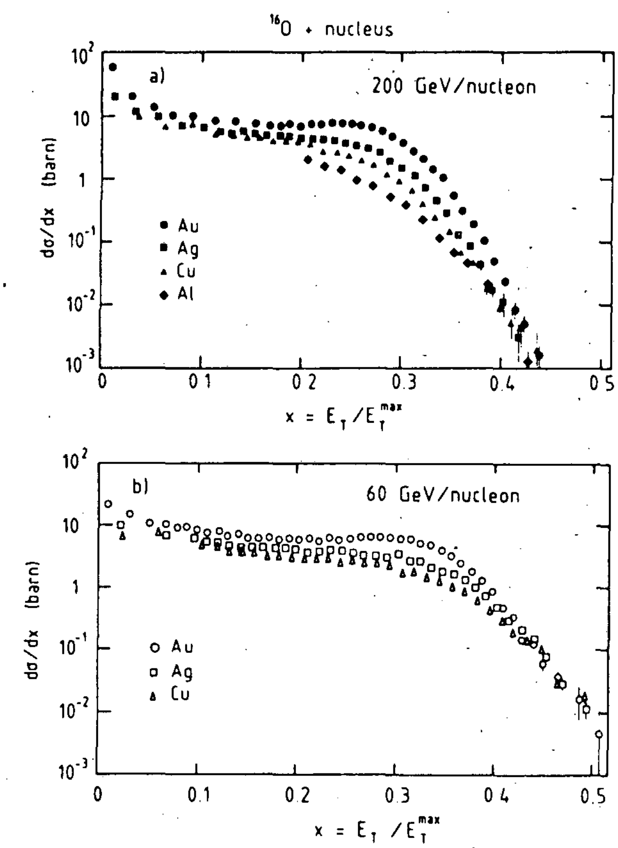

Fig. 23

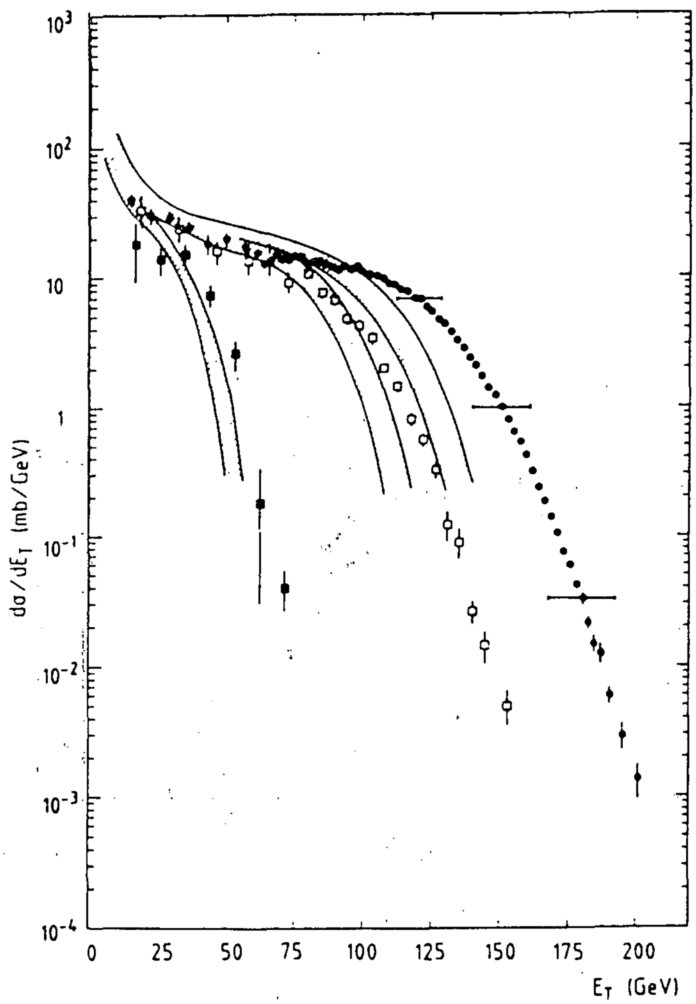

Fig. 24

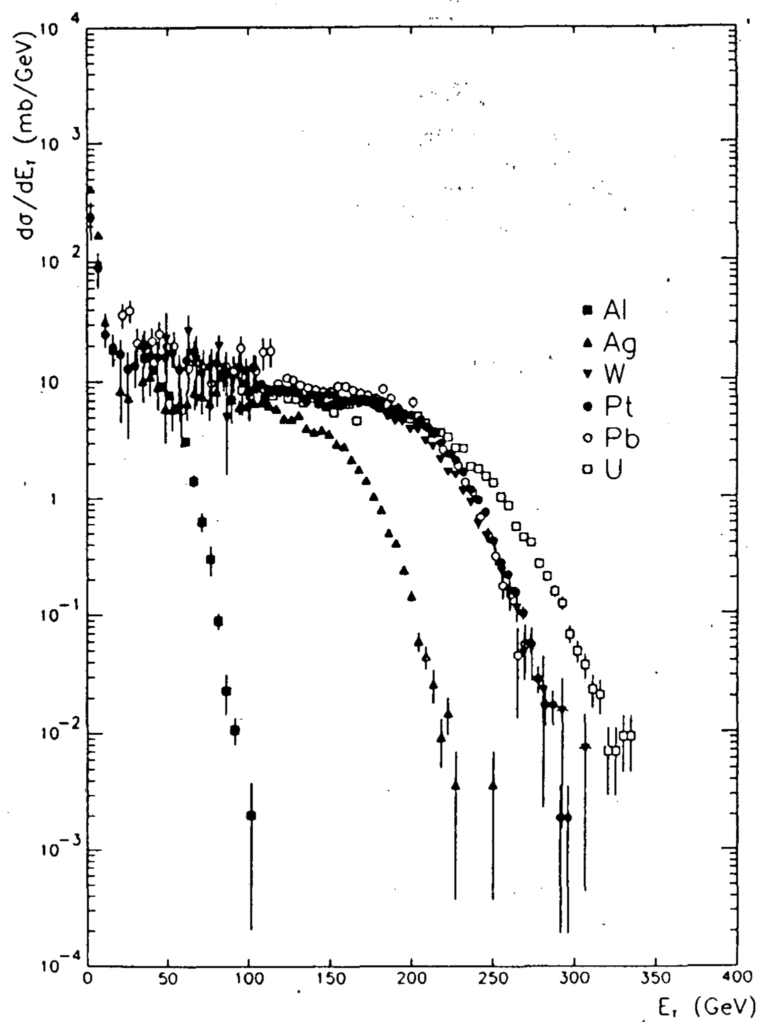

Fig. 25

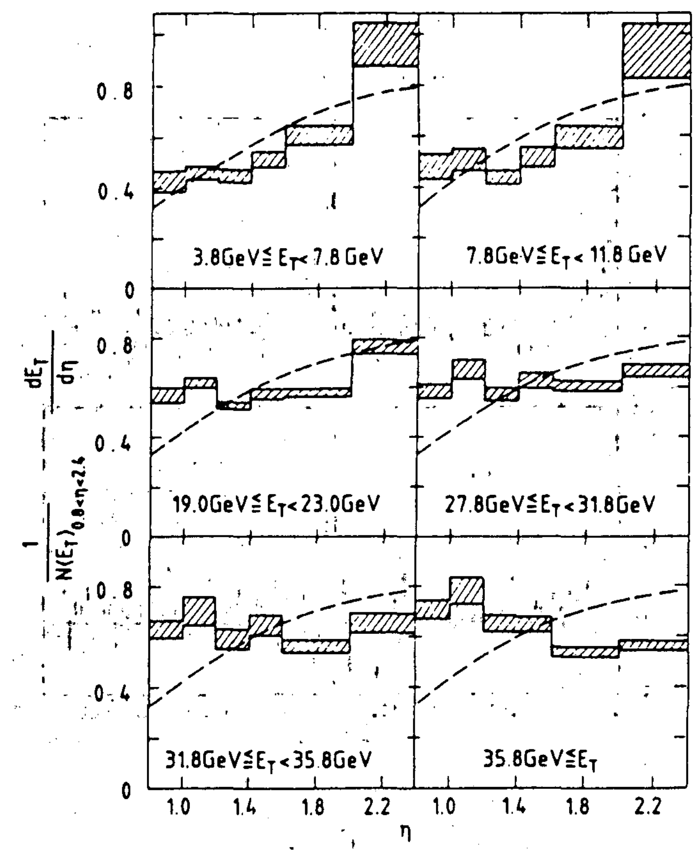
3.8GeV≦E_T<7.8GeV
7.8GeV≦E_T<11.8GeV
19.0GeV≦E_T<23.0GeV
27.8GeV≦E_T<31.8GeV
31.8GeV≦E_T<35.8GeV
35.8GeV≦E_T
1/N(E_T)_0.8<η<2.4 · dE_T/dη
η

Fig. 26

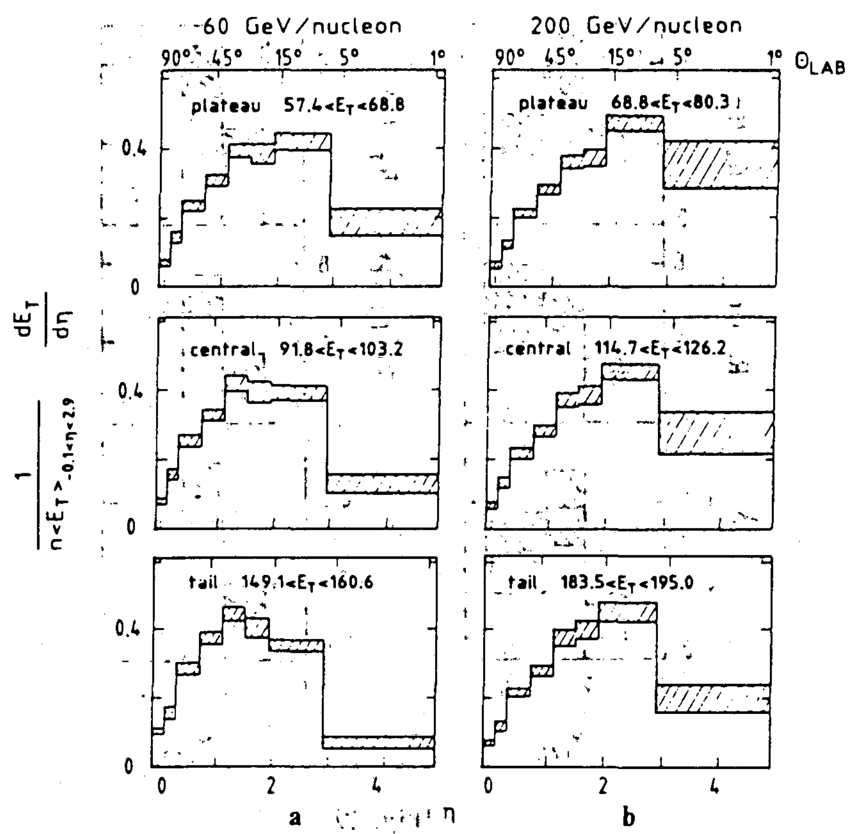
60 GeV/nucleon
200 GeV/nucleon
Θ_LAB
plateau 57.4<E_T<68.8
plateau 68.8<E_T<80.3
central 91.8<E_T<103.2
central 114.7<E_T<126.2
tail 149.1<E_T<160.6
tail 183.5<E_T<195.0
1/n<E_T>_-0.1<η<2.9 · dE_T/dη
a
b
η

Fig. 27

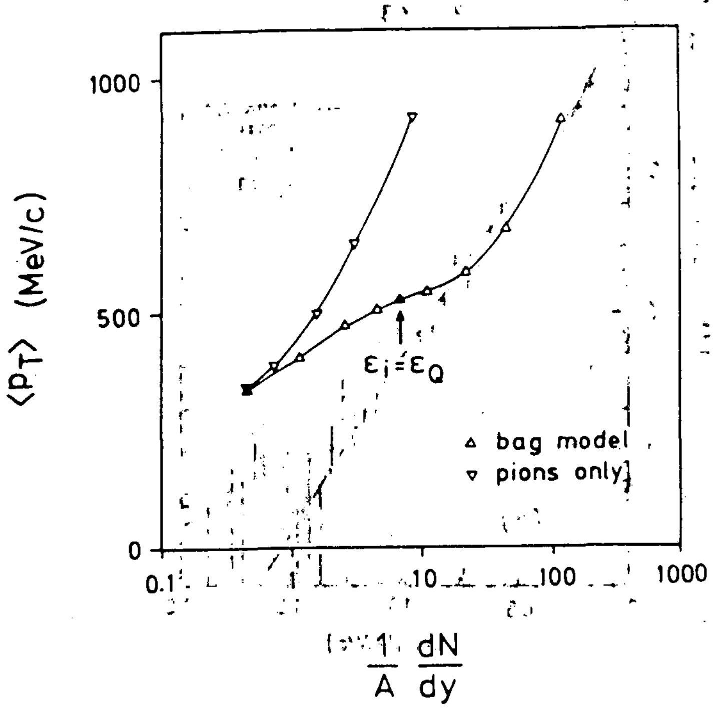
1000
500
0
0.1
1
10
100
1000
⟨p_T⟩ (MeV/c)
$\varepsilon_i = \varepsilon_Q$
bag model
pions only
$\frac{1}{A}\frac{dN}{dy}$

Fig. 31

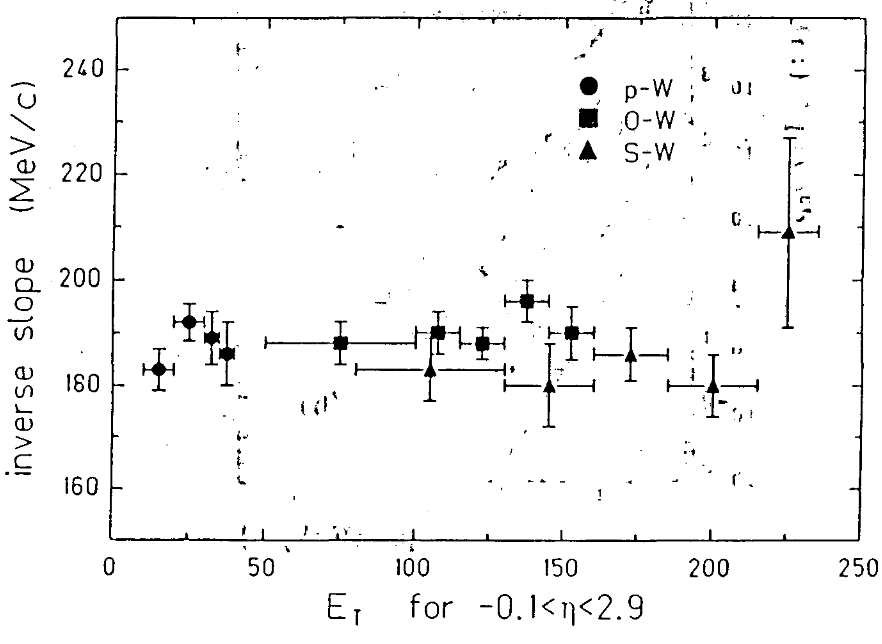
p-W
O-W
S-W
240
220
200
180
160
0
50
100
150
200
250
inverse slope (MeV/c)
E_T for $-0.1<\eta<2.9$

Fig. 32

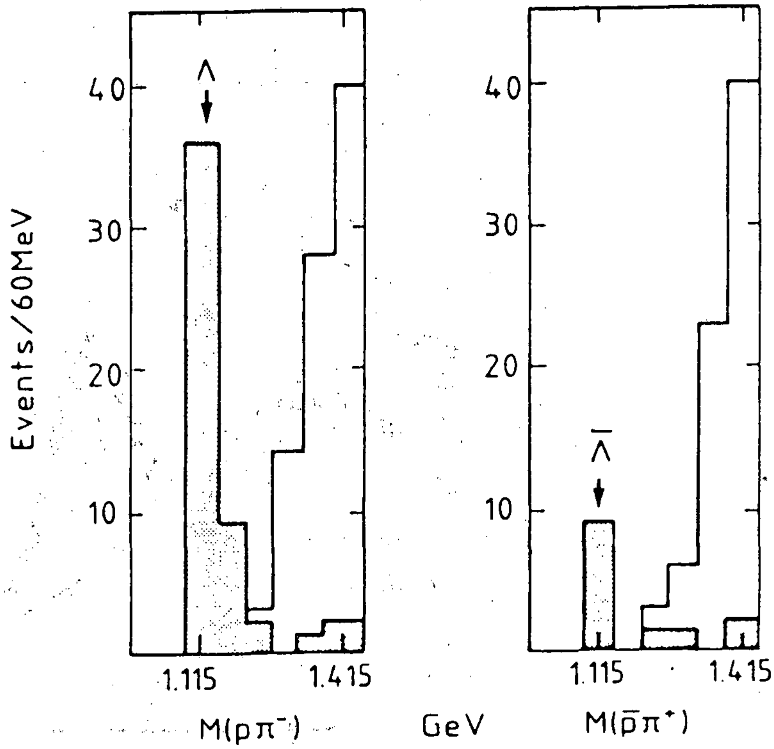
Λ
$\bar{\Lambda}$
Events/60MeV
40
30
20
10
1.115
1.415
M(pπ⁻)
GeV
M(p̄π⁺)

Fig. 33

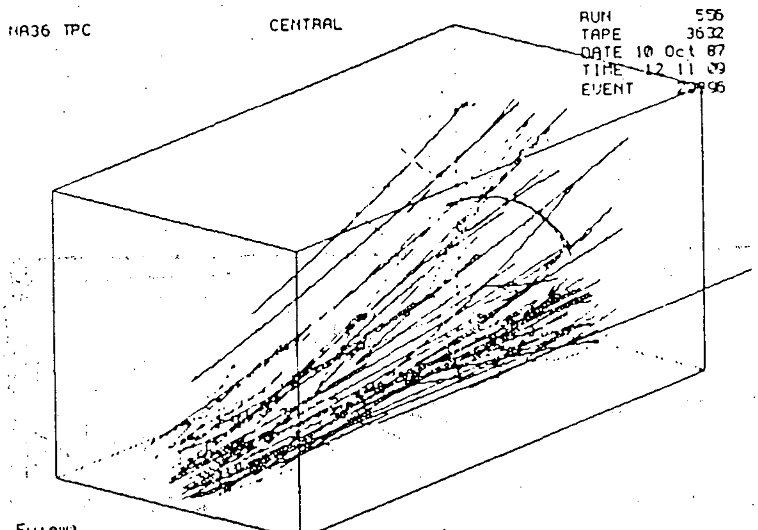
NA36 TPC
CENTRAL
RUN 556
TAPE 3632
DATE 10 Oct 87
TIME 12 11 09
EVENT 29896
Eview>

Fig. 34

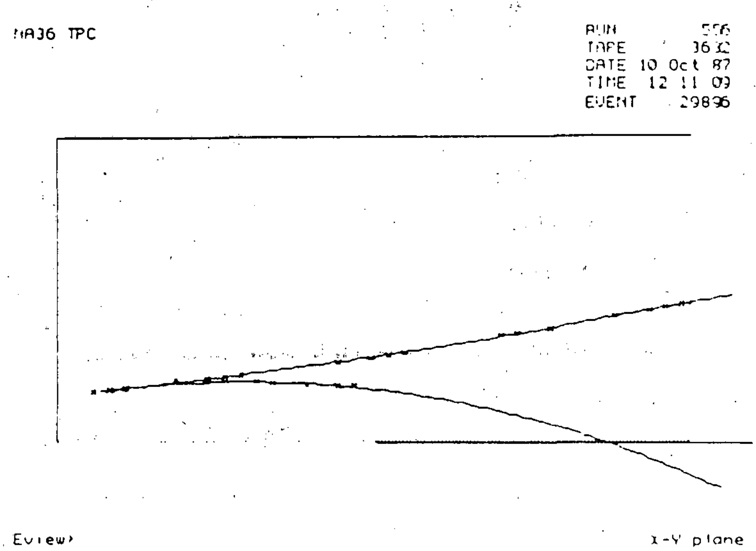
NA36 TPC
RUN 556
TAPE 3632
DATE 10 Oct 87
TIME 12 11 09
EVENT 29896
Eview>
X-Y plane

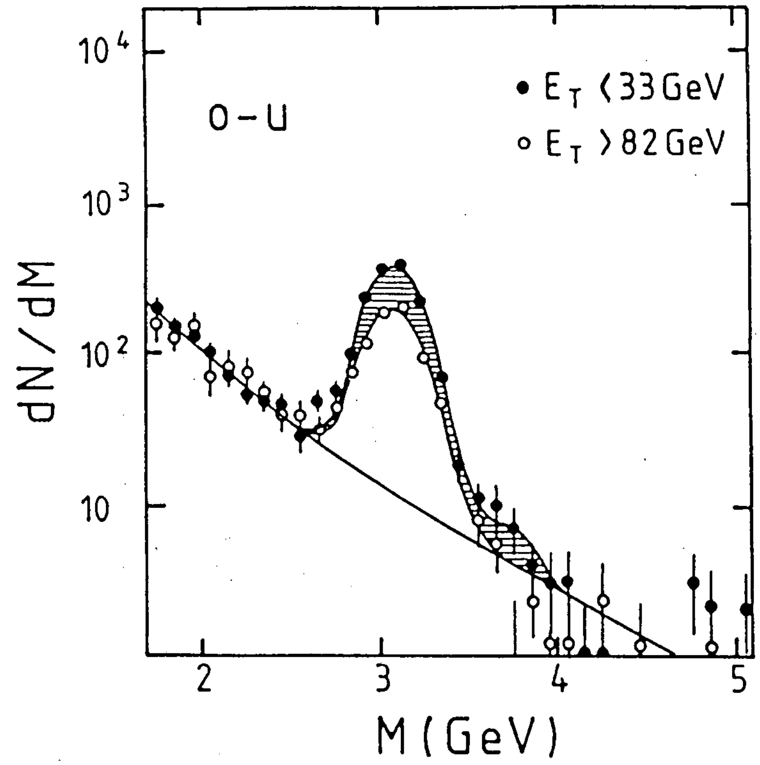

10^4
10^3
10^2
10
O – U
• E_T ‹33 GeV
○ E_T ›82 GeV
dN/dM
2
3
4
5
M (GeV)

Fig. 35

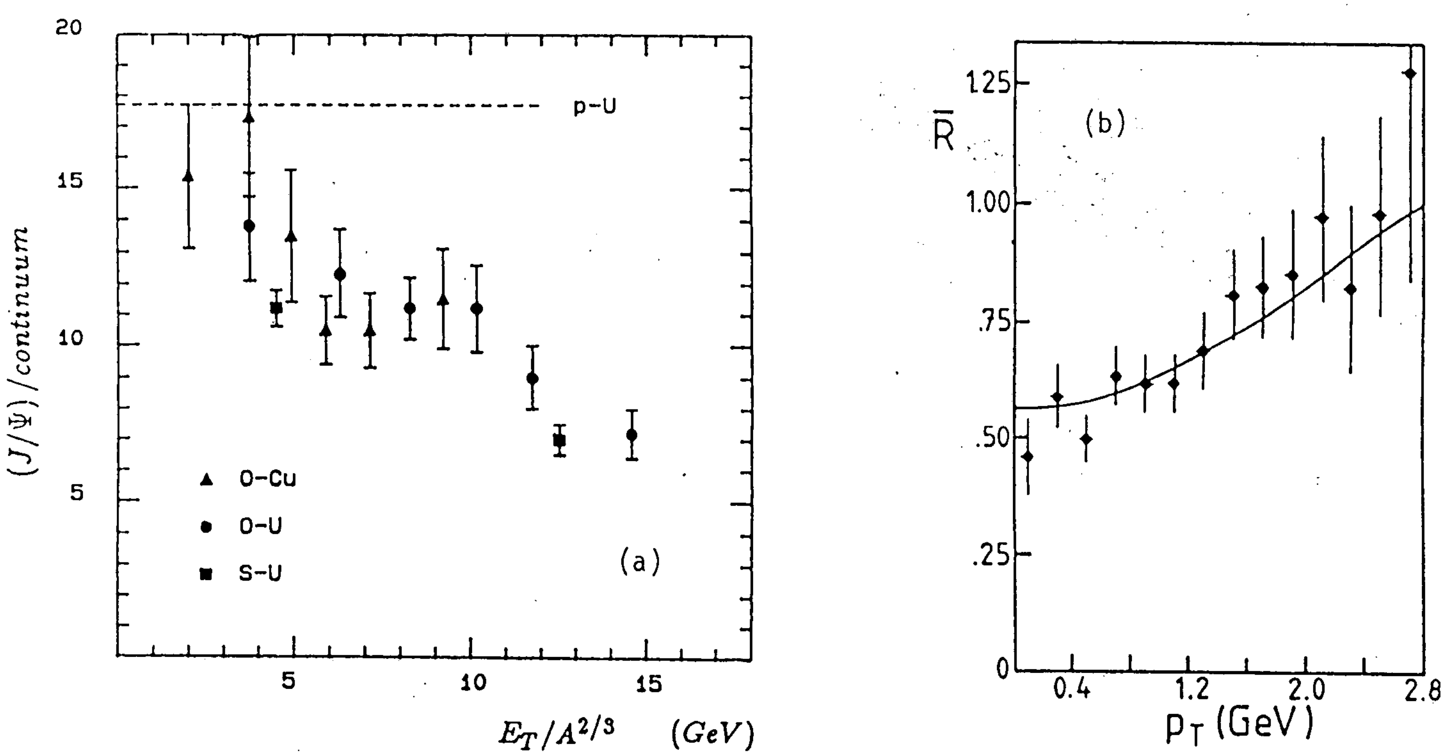

20
15
10
5
p-U
O-Cu
O-U
S-U
(a)
(J/Ψ)/continuum
5
10
15
E_T/A^{2/3} (GeV)
1.25
1.00
.75
.50
.25
0
R̄
(b)
0.4
1.2
2.0
2.8
p_T (GeV)

Fig. 36

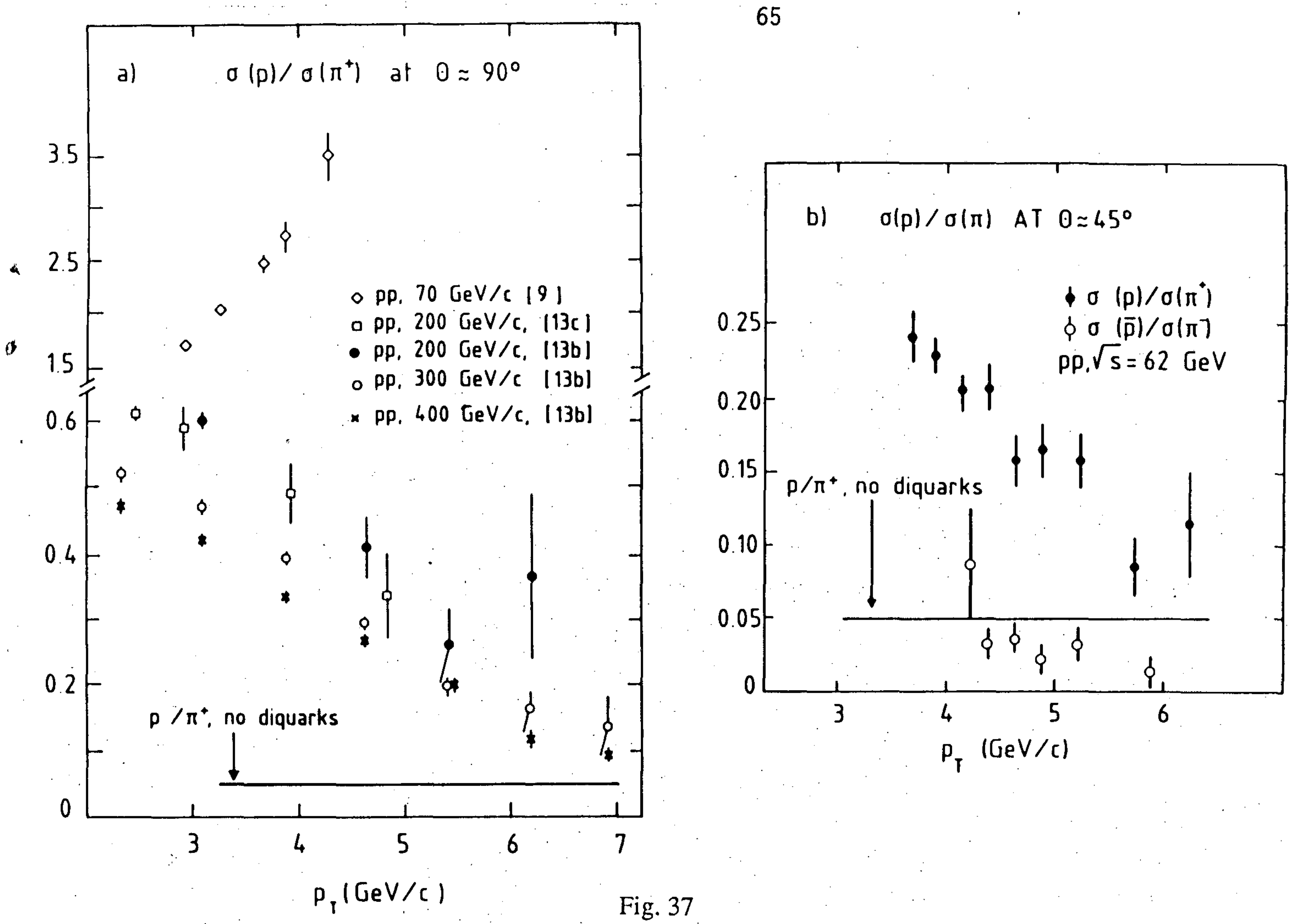

a) σ (p) / σ (π⁺) at Θ ≈ 90°
3.5
2.5
1.5
0.6
0.4
0.2
0
◇ pp, 70 GeV/c [9]
□ pp, 200 GeV/c, [13c]
● pp, 200 GeV/c, [13b]
○ pp, 300 GeV/c [13b]
* pp, 400 GeV/c, [13b]
p / π⁺, no diquarks
3
4
5
6
7
p_T (GeV/c)
b) σ(p) / σ(π) AT Θ ≈ 45°
σ (p)/σ(π⁺)
σ (p̄)/σ(π⁻)
pp, √s = 62 GeV
0.25
0.20
0.15
0.10
0.05
0
p/π⁺, no diquarks
3
4
5
6
p_T (GeV/c)

Fig. 37

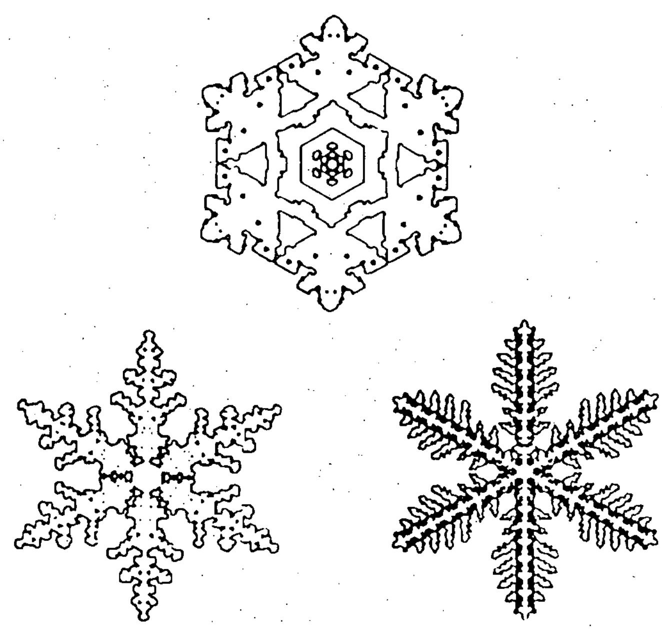

Fig. 38

LAWRENCE BERKELEY LABORATORY
TECHNICAL INFORMATION DEPARTMENT
1 CYCLOTRON ROAD
BERKELEY, CALIFORNIA 94720